HHS Public Access

Author manuscript

Curr Biol. Author manuscript; available in PMC 2024 August 21.

Published in final edited form as:

Curr Biol. 2023 August 21; 33(16): 3465–3477.e5. doi:10.1016/j.cub.2023.07.021.

Anti-Hebbian plasticity in the motor cortex promotes defensive freezing

Yang Bai[1], **Bryce Grier**[1], **Erez Geron**[1,2,*]

[1]Neuroscience Institute, New York University, New York, New York 10016

Summary

Regional brain activity often decreases from baseline levels in response to external events, but how neurons develop such negative responses is unclear. To study this, we leveraged the negative response that develops in the primary motor cortex (M1) after classical fear learning. We trained mice with a fear conditioning paradigm while imaging their brains with standard two-photon microscopy. This enabled monitoring changes in neuronal responses to the tone with synaptic resolution through learning. We found that M1 layer 5 pyramidal neurons (L5 PNs) developed negative tone responses within an hour after conditioning, which depended on the weakening of their dendritic spines that were active during training. Blocking this form of anti-Hebbian plasticity using an optogenetic manipulation of CaMKII activity disrupted negative tone responses and freezing. Therefore, reducing the strength of spines active at the time of memory encoding leads to negative responses of L5 PNs. In turn, these negative responses curb M1's capacity for promoting movement, thereby aiding freezing. Collectively, this work provides a mechanistic understanding of how area-specific negative responses to behaviorally-relevant cues can be achieved.

Abstract

Bai *et al.* visualize activity in the motor cortex during and after fear conditioning to understand negative neuronal responses. They find that such negative responses (when neuronal activity drops below baseline), and defensive freezing responses, depend on the weakening of dendritic spines that were active during conditioning

Graphical Abstract

*Correspondence: Erez.geron@nyulangone.org.
[2]Lead contact

Author contributions:
EG., and YB., designed, performed, and analyzed the data; BG. analyzed the data; EG. wrote the paper.

Declaration of interests:
The authors declare no competing interests.

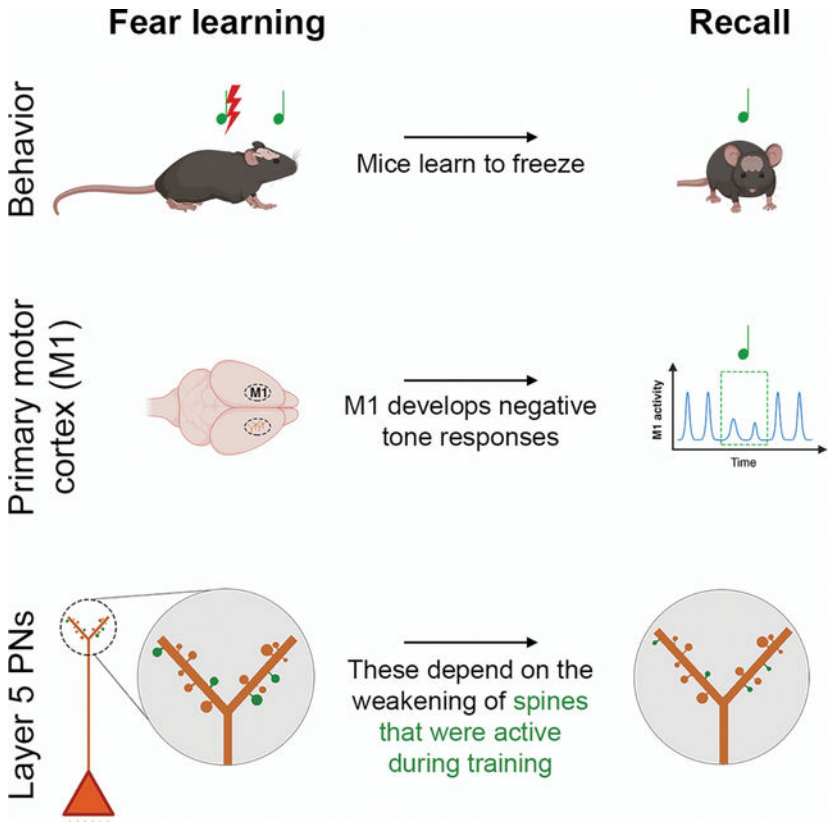

Introduction

Usually, we think of a response as an action that follows a signal, but such a definition leaves out negative responses: instances where an action is specifically not taken. In lab animals, whose behavior heavily corresponds with movement, defensive freezing, where animals stay still upon a threatening signal, can be thought of as a negative behavioral response (see Video S1). The broad distinction between positive and negative responses also applies to regional neuronal activity, which can increase or decrease from baseline levels in response to a stimulus or during behavioral actions.[1–3] Indeed, negative neuronal responses are less intuitive and less well-studied than positive ones, yet there is ample evidence that negative neuronal responses are a common feature of brain activity. For example, negative regional responses are involved in perception of stimuli from various modalities,[1,2,4] body movements,[5] and higher cognitive functions such as word comprehension[6,7] and decision-making.[8] Furthermore, negative responses are disrupted in disease.[8,9] Since negative neuronal responses are typically studied using imaging tools with limited resolution, such as fMRI and PET, our understanding of their underlying mechanisms is also limited.

Defensive freezing behaviors involve negative neuronal responses in the primary motor cortex (M1),[10–13] concomitant with positive responses in the lateral amygdala, auditory cortex, and periaqueductal gray.[11,14–17] M1 is a frontal cortical region that controls voluntary movements together with other motor-related brain structures,[18–20] and its activity is anticorrelated with freezing behavior.[10–12] One possible explanation for the reduction

in M1's activity upon freezing is that it results from the freezing itself (i.e., the lack of movement). Indeed, activity in M1 covaries with many movement parameters, including timing, trajectory, kinematics, and force.[18] However, this does not rule out that M1's negative responses during freezing reflect an inherent reduction of activity that is partly independent of freezing. At the cellular/circuit levels, negative responses to a cue could result from (1) more inhibitory input onto excitatory neurons by GABAergic interneurons (INs);[3,21,22] (2) less excitatory input onto excitatory neurons (a pre-synaptic mechanism); or (3) reduced responsiveness to the cue by the excitatory neurons themselves (a post-synaptic mechanism). We will argue that the latter mechanism is prevalent in M1 upon fear learning, and that this acquired reduction of M1 activity is critical for reinforcing freezing behavior.

Freezing is also the primary readout of the classical fear conditioning paradigm, a heavily used tool in studying learning and memory. This paradigm typically involves pairing a tone with an aversive stimulus (e.g., electric foot shock). After the first tone-shock pairing, animals regard the tone (now the conditioned stimulus) as a predictor of the shock and freeze to its sound.[16,23–25] The extent of freezing response (the percentage of tone time spent freezing) indicates memory strength.

Here, we studied negative responses in M1 that support defensive freezing. We first verified that M1 is essential for acquiring conditioned freezing. We then employed standard two-photon microscopy during and after fear conditioning to examine neuronal tone responses in M1. We found that layer 5 pyramidal neurons (L5 PNs; the principal cortical output cells) developed a negative tone response without a positive response from the INs that inhibit them (i.e., L5 PV, L5 SST, and L1 NDNF INs). Notably, during training, L5 PNs' dendrites and spines exhibited a transient positive tone response that shifted into a negative one within an hour. Spines that were active during training became smaller and less active at later recalls, which are clear indications of spine weakening.[26–29] Furthermore, blocking the weakening of spines active during training by inhibiting CaMKII activity disrupted negative responses and freezing. Thus, we identified a form of anti-Hebbian plasticity,[30–32] where the weakening of spines active during training/encoding supported later negative responses and freezing behaviors.

Results

Fear learning under the microscope and a in box and its dependence on M1

We wanted to harness the sensitivity of two-photon microscopy to visualize the acquisition of negative tone responses in M1. Therefore, we constructed a conditioning plate with which mice were trained during imaging (Figure S1A). To test how the freezing responses of animals trained while head-restrained fit with more standard training regimes, we compared the freezing responses of mice trained under a microscope to those trained in a conditioning box. In each setting, we trained the mice with one of three protocols: a single tone-shock pairing, two pairings, or with a non-associative control protocol where the shock preceded the tone by eight seconds (Training: tone: 20 s, 4 kHz, 75 dB; shock: 2 s (co-terminating with tone in associative protocols); 0.3 or 0.5 mA (box and plate, respectively) (Figures 1A; S1B, C). For all animals (in this and the subsequent figures), freezing responses were tested at a 24 h recall test in a conditioning box where the animals were freely

moving (Recall: tone: 4 kHz, 75 dB, 120 s) (Figure 1B). Freezing levels in animals trained under the microscope were significantly lower than those trained freely moving (Figures 1C, D), which agrees with other work.[33,34] We found that these lower freezing levels resulted partly from the head-holder placement surgery that naïve animals did not undergo (Figure 1E). Low freezing levels of animals trained under the microscope were partially ameliorated by habituation to the recall environment, and by performing recall in quieter conditions (Figure S1E). As the differences between these settings are large and include differences in the training conditions and the state of the animals (surgery vs. naïve), we find the best comparison to be between animals trained with different protocols in the same settings. When the freezing responses in each setting were compared across the training protocols, similar phenomena emerged: learning was evident only after associative training, and training with two parings yielded more freezing than with a single pairing (Figures 1C, D).

We next tested a fourth protocol, where the second shock was omitted (i.e., the pairing + tone protocol) (Figure 1A). Notably, in both training settings, this protocol yielded higher freezing responses at recall than training with a single pairing (Figures 1C, D). Presentation of a non-reinforced tone may be expected to erode the tone-shock association. However, it is established that extinction sessions do not extinguish long-term fear responses when administered shortly after training (the immediate extinction deficit).[35,36] Since the pairing + tone protocol yielded relatively high freezing levels, subjected the mice to fewer shocks, and simplified the analysis of event-related activity, it was used as our primary training protocol. Overall, we found that training under a microscope yields fear learning.

The primary motor cortex is required for the acquisition of conditioned freezing

We next tested if M1 is required for acquiring conditioned freezing. For that, we expressed the optogenetic silencer, ArchT (or EGFP in controls) in PNs of M1 (Figure 1F). Three weeks later, mice were implanted with optical fibers above M1, and training in a conditioning box commenced four days afterward. Light (565 nm) was applied during the second tone to inactivate M1 in ArchT-expressing mice (Figure 1F'). Notably, inactivation of M1 during the second tone disrupted conditioned freezing in the 24 h recall test (Figure 1G).[13] In addition, in a second control group, M1 of ArchT-expressing mice was inactivated after a 10 minute delay. Animals of this group did not exhibit reduced freezing levels compared to EGFP-expressing animals, which shows that ArchT expression did not compromise learning by itself (Figure 1G). Together, we found that fear acquisition is dependent on M1.

M1 L5 PNs develop negative tone responses without concomitant positive responses from INs that inhibit them

Next, we tested how neuronal tone responses in M1 change through fear learning by imaging Ca^{2+} activity during training with the pairing + tone protocol and at a 4 h recall test (Figure 2A). These animals were tested for freezing levels (in a box) a day after training (Figures S1G, H). Since training under the microscope failed to yield any freezing in many animals, we focused our analyses (Figures 2, S2) on animals with freezing scores above the median and a more than two-fold increase in freezing in response to the tone (good learners were

significantly distinct from bad learners: $\chi^2(1) = 57.947$, $p < .001$, Kruskal-Wallis test, n= 40 good and 48 bad learners; see methods and Figure S1H. For Ca^{2+} analysis of good and bad learners see Figure S2). We surveyed the activity changes of several neuronal types in the caudal forelimb area of M1.[37] Specifically, imaging focused on L5 PNs and on INs that preferentially inhibit their soma or apical dendrites. For the visualization of L5 PNs, we used a *Thy1*::GCaMP6s line (500–650 μm below the pia for somata and 20–70 μm for apical dendrites).[38] We visualized Ca^{2+} activity of three types of inhibitory INs: L5 PV (soma-targeting), L5 SST (dendrite-targeting), and L1 NDNF (dendrite-targeting) (Figure 2B).[39,40] To this end, we used cell-type specific transgenic Cre animals (e.g., *PV*::Cre), injected with AAVs harboring a Cre-dependent GCaMP6s construct. Finally, freezing levels were measured in a conditioning box 24 h after training.

During training and recall we observed several broad response types in the above-mentioned INs. First of all, there were no significant tone responses prior to the shock, except for an increase in Ca^{2+} activity of NDNF INs (Figures 2C, D). Second, the activity level of all cell types increased following the shock, save for SST INs (Figures 2C, D; S2), and PV INs exhibited a pronounced step increase in activity (Figures 2C, D; S2D‘). We also observed that tuft dendrites exhibited increased activity to the tone presented during training after the shock (Figures 2C, D; Video S2). This dendritic positive tone response coincided with decreased activity of SST INs. Furthermore, as expected,[10–13,24,41] dendrites and somata of L5 PNs exhibited a negative tone response at the 4 h recall test (Figures 2C, D; Video S3). Finally, INs did not exhibit significant positive or negative tone responses at the 4 h recall test (Figures 2C, D).

Negative responses in M1 support freezing

As introduced above, the negative tone responses of L5 PNs could be the cause and/or result of freezing. To better understand the relationships between negative responses in M1 and freezing, we imaged recall tone responses of L5 PNs of head-restrained mice while monitoring their gross body movements with an infrared camera. To minimize contextual responses to the imaging/training arena (such as a low basal activity), we trained these animals in one box and verified freezing responses in a different box a few hours before imaging (freezing before tone: 17 ± 6.04 %; freezing during tone: 54.8 ± 12.2 %; mean ± SEM; p= 0.008; n= 5 animals; paired t-test. Gross body movements were calculated by measuring its centroid’s displacement (see methods).

Measuring gross body movements of head-restrained animals and correlating these with activity in M1 may be problematic for understanding actual freezing, since the nature of the behavioral responses of head-restrained animals at recall is unclear, and as even freely-moving animals do not always freeze instantly to the tone (Video S1). Indeed, here, head-restrained animals did move at recall (Figure 3A, pink trace, average movement and SEM in five animals). Nevertheless, this experiment was informative, as it provided qualitative observations, where M1 activity rapidly decreased upon tone presentation before a reduction in body movements or even irrespective of it (Figure 3B; two of three examples). This mismatch between M1’s negative responses and movements suggests that freezing itself is not a prerequisite for negative responses in M1.

We sought a different setting to test the relations between negative responses in M1 and freezing. We reasoned that if freezing is independent of M1's activity, then artificially increasing M1's activity would not affect freezing levels. Therefore, we tested the effects of elevating M1 L5 PN activity on freezing, using the Gi-DREADD-CNO system to reduce cortical inhibition. To achieve this, we injected PV-Cre mice in M1 with viruses harboring a Cre-dependent Gi-DREADD construct and imaged GCaMP activity in PNs (Figure 3C). We verified separately that in animals expressing Gi-DREADD in PV INs and a GCaMP probe in PNs, administering CNO did indeed increase the activity of adjacent PNs as compared to control animals (injected with tdTomato instead of the Gi-DREADD) (1.2. ± 0.1 and 4.2 ± 0.6 mean ± SEM fold increase in activity after CNO; 5 animals in the control and experimental groups; p= 0.002; unpaired t-test). We then conditioned PV-Cre animals expressing either Gi-DREADD or GFP without manipulating their M1 activity. However, at the recall test a day later, animals were administered CNO to activate M1 in the experimental group (Figure 3C'). Notably, we found that mice whose M1 was disinhibited at recall exhibited less freezing than control mice (Figure 3D), indicating that negative responses in M1 support freezing.

Emergence of negative tone responses of L5 PNs during associative learning

The dendritic response to the tone of L5 PNs in M1 was positive at early stages of learning (2^{nd} tone presentation, 90 s after tone-shock pairing) and negative 4 h later (Figures 2C, D; S2; Videos S2, S3). To assess when the dendritic responses to the tone changes from positive to negative, we performed a control experiment in which we imaged dendritic tone responses at different intervals after training (Figure S3A). Specifically, *Thy1*::GCaMP6s animals were trained under the microscope with a single pairing and presented with the tone during re-imaging 15, 30, or 120 minutes later (Figure S3A). Here, a positive tone response was apparent 15 minutes after the first pairing, and this response changed to being negative within two hours (Figure S3B). These results indicate that a single tone-shock pairing was sufficient to induce dendritic negative responses, as early as 2 h after training. In line with previous work,[10,11] somatic activity at the 4 h recall test correlated negatively with freezing a day later (R= −0.64; p= 0.017; n= 13 animals).

We next used WT mice with sparse, AAV-mediated double-labeling. Here, the PNs expressed the cytosolic structural marker tdTomato and the Ca^{2+} probe GCaMP6s. This combination of marker of structure and activity was essential for tracking the dendrites' corresponding soma and identifying the cell's layer location, assuring the stability of imaging of dendrites, and for measuring spine structural plasticity (Figures 4A–B'). Mice bearing sparsely labeled PNs were subjected to two recall tests, 1 and 8 h after training, to allow for monitoring of spine plasticity in relevant time scales (see Figure 5).[26–29] In agreement with the results obtained in *Thy1*::GCaMP6s animals, dendrites of double-labeled L5 PNs exhibited a positive tone response during training and a negative response at the recall tests (Figures 4C, D; Video S4). However, sparse labeling provided the advantage of re-imaging the same dendrites and their soma and revealed that neurons whose dendrites were more active during training were more likely to exhibit negative tone response at recalls (Figure 4E; Video S4).

Finally, we tested the responses of L5 PNs during and after training with the non-associative protocol (unpaired + tone). Notably, non-associative training yielded dendritic tone responses distinct from those observed in associative training: dendrites did not exhibit positive and negative responses at training and recall, respectively (Figures 4F, G; S4A, B; Video S5). In addition, dendritic and somatic responses at recall tests were heterogeneous and did not correlate with the dendritic response during training (Figures 4F–H; S4A, B; Video S5). Collectively, most M1 L5 PNs displayed a positive dendritic tone response during associative training and negative responses at later recalls. Cells with a strong initial response to the tone were more likely to exhibit a negative response later, suggesting that these inverse responses are linked.

Persistent weakening of dendritic spines that were active during training

The finding that apical dendrites develop a negative tone response in the absence of any increased activity of the inhibitory INs that inhibit them (Figure 2) suggests that synaptic plasticity in these dendrites may underlie the acquisition of negative responses. Synaptic plasticity is known to be affected by dendritic Ca^{2+} spikes, which were abundant after the shock application (Figures 2C, D; 4C, D).[42–44] We therefore took advantage of the high sensitivity of imaging in head-restrained animals to visualize dendrite and spine activity at training and recall, and assessed changes in Ca^{2+} responses and spine size. The latter correlates positively with post-synaptic strength, and the change in spine size is a well-established proxy for post-synaptic plasticity.[26–29]

Mice bearing sparse labeling of PNs were trained with the pairing + tone protocol and subjected to 1 and 8 h recall tests (as in Figure 4). Imaging focused on L5 PN dendrites, and their spines, located in L1. By using non-negative matrix factorization (NMF) to cluster the activity traces of spines, we detected two significant patterns of spine activity during training. Spines in cluster one, which contained approximately two-thirds of the spines (144/210 spines; 9 neurons), exhibited a rapid increase in activity following the shock, which peaked at ~20 s following the shock (Figure 5A). In contrast, the spines in cluster two did not exhibit a response to the shock, and their activity ramped up later, reaching its peak after the second tone (Figure 5A). We did not find significant differences between the clusters in initial spine size or in several activity measures (Figures S5A–D). Next, we measured spine activity during the 1 and 8 h recall tests. Across the spine population, we identified negative tone responses at both time points (Figures 5A, C). Significantly, the spines' tone responses at each recall were negatively correlated with their maximal activity during training (1h: $R = -0.21$, $p = 0.0028$, $n = 192$ spines; 8h: $R = -0.28$, $p = 0.004$, $n = 149$ spines; 9 cells) (Figure 5D).

Following this, we performed the same analyses for spine activity during training with the unpaired + tone protocol. Superficially, clustering non-associative training data revealed similar patterns to associative learning: we found two significant spine activity clusters where one cluster exhibited increased activity after the shock and the other increased its activity further into training (Figure 5B). However, we did not find a negative spine response at recall, and activity during training did not predict responses at recall (Figures 5F, G). These results suggest that the negative responses observed in the pairing + tone protocol are

not a general response of spines with high activity during training, but rather a characteristic of associative fear learning in M1.

We then assessed spine plasticity by measuring spine size changes, for which we acquired high-resolution images of dendrites and spines before training and recall tests (Figure S6). Using this indicator of plasticity, we again found evidence for the weakening of spines that were active during associative learning. Specifically, spines size change was negatively correlated with activity during associative training but not with activity during non-associative training (associtiave:1h: R= −0.23, p= 0.0007, n= 210 spines; 8h: R= −0.15, p= 0.039, n= 173 spines; 9 cells) (Figures 5E, H). Interestingly, following associative training, spines in cluster two showed a greater initial reduction in size compared to cluster one, a trend that equalized 8 h after training (Figure S5E). Finally, we found that spine size change was also negatively correlated with initial spine size (associative: R= −0.18; p = 0.008; n= 210; 8h: R= −0.24; p= 0.001; n= 173; 9 cells. Non-associative: 8h: R= −0.46; p< 0.0001; n= 70; 3 cells) (Figures 5I, K). As we did not find a correlation between spine activity during training and initial spine size (Figures 5J, L), these findings may indicate slow-acting homeostatic processes that limit spine size independently of activity [43]. Overall, analyses of spine data showed an inverse correlation between spine activity during associative learning and plasticity, reminiscent of anti-Hebbian plasticity (weakening of synapses that contributed to firing).[30–32]

Disruption of CaMKII-dependent spine plasticity perturbed the acquisition of negative tone responses and conditioned freezing

The results above indicate a correlation between synaptic weakening of learning-related spines and negative tone responses of L5 PNs. To test causality, we sought to manipulate spine plasticity after training and assess the effect on neuronal and behavioral responses to the tone. To do this, we employed transient optogenetic inhibition of CaMKII, a Ca^{2+}-dependent master regulator of spine plasticity that is involved in several types of long-term depression (LTD), including anti-Hebbian plasticity.[45–47] Inhibition was achieved using a LOV2-based inhibitor (paAIP2), which upon exposure to blue light, binds to active CaMKII and prevents it from activating downstream effectors (Figure 6A).[48] We used mice with sparse double-labeling of paAIP2-CyRFP and GCaMP6s in M1 L5 PNs to minimize any disruption of the local circuit (Figure 6B). CaMKII activity was inhibited by applying blue light (470 nm) for 15 s immediately after the second tone or after a ten-minute delay in control animals. This paAIP2 illumination protocol has been shown to inhibit CaMKII during the illumination and subsequent 45 s.[48] To control for the different timing of illumination between the immediate and delayed inhibition groups, a control light (565 nm) was applied at matching time points (Figure 6C).

During training, dendritic and synaptic activity in the control and experimental neurons were similar to one another (Figures 6D, E). As expected, CaMKII inhibition during training, a period sensitive to perturbations (Figures 1F–G), had a pronounced effect on the spines' structural plasticity (Figure 6F). Spines in the delayed inhibition group exhibited a negative correlation between spine activity at training and structural plasticity (R= −0.27; p= 0.002; 117 spines) (Figure 6F). However, spines in the immediate inhibition group did not exhibit

a negative relation (R= 0.03; p= 0.67; 143 spines), and their plasticity pattern differed significantly from that of the delayed inhibition group ($F_{1, 256}$= 5.45; p= 0.02; One-way ANCOVA) (Figure 6F). Most importantly, dendrites and somata in the immediate inhibition group, where plasticity was abnormal, did not exhibit negative tone responses, supporting a role for weakening of learning-related spines in mediating negative responses to the tone (Figure 6G; Video S6).

Finally, we tested the effect of CaMKII inhibition on conditioned freezing. For this, we used mice in which paAIP2 was densely expressed in M1 (Figure 6H inset). Here, the mice were trained with either the pairing + tone or the two-paring protocol. CaMKII activity was inhibited after the second tone (or tone/shock pairing) or 10 minutes later (Figure 6B), and freezing was measured 24 h after. Notably, after training with both protocols, animals of the immediate CaMKII inhibition group did not display increased freezing to the tone (Figure 6H). In sum, our findings show that negative plasticity of spines that are active during training is essential for negative tone responses in M1 and conditioned freezing.

Discussion

We investigated how neurons can develop a negative response to an external stimulus by studying negative tone responses in M1 following fear conditioning.[10–13] We found that the acquired negative tone response of M1 L5 PNs depended on the selective weakening of excitatory spines. Spines that were active during training displayed a lasting reduction in size and negative tone responses (Figure 5). Furthermore, disrupting spine dynamics by inhibition of CaMKII activity, a master regulator of spine plasticity, impaired the acquisition of negative tone responses, and conditioned freezing behavior (Figures 6F, G).

To simplify the analysis of stimulus-related neuronal activity we used a minimal training protocol consisting of a single tone-shock pairing followed by a second presentation of the tone. A presentation of a non-reinforced tone may raise the question of whether it could compromise learning. Multiple lines of evidence indicate that this is not the case, however. First, fear extinction cannot be initiated during such early stages of learning, a phenomenon known as the immediate extinction deficit.[35,36] Second, as mice froze to the second, non-reinforced tone (Figures S1B, C), it is likely that the animals had already formed an initial association between the tone and shock at that time. Therefore, during the second presentation, the animals processed the tone in the context of the shock. It is akin to the testing effect, where retrieval of recently encoded information improves its long-term retention (better than being re-taught).[49] The similarity is that in the absence of the shock, the animal is not re-experiencing the original pairing but processes it, as in the testing effect, where subjects are not being re-taught but are asked to recall the recently learned material. These peri-encoding mechanisms do not create the memory trace but elaborate it, contextualize it, and create additional retrieval routes to it.[50,51]

We inspected the activity of L5 PNs and INs from different classes that inhibit the soma or dendrites of PNs. Notably, we did not observe the acquisition of either positive or negative responses overall in any IN class. It is possible that distinct IN subpopulations within each class might exhibit specific responses that are obscured by the overall population. For

example, it was shown that distinct subgroups of SST[52] and PV[53] INs operate differentially during fear learning in the prefrontal cortex. Anecdotally, some of our results indicate differential activity of M1 SST INs (see the opposing changes in activity of two SST populations during recall Figure 2C). It would be interesting to parse INs into functionally defined groups and examine whether these populations correspond to distinct genetic subtypes. We do note, however, that the increase in PN dendritic activity during and following the second tone coincided lower activity in dendrite-targeting INs (Figures 2C, D). This increase in dendritic activity may be facilitated also by long-range modulatory signaling. In 2017, LeDoux and colleagues demonstrated that training with two pairings induced more freezing than with a single pairing. They found that this second pairing-dependent improvement of learning could be inhibited by blocking adrenergic signaling.[54] The second tone in our setup may be enough to induce adrenergic recruitment, which in turn could increase dendritic activity in L5 PNs.[55]

The most well-studied synaptic mechanism of associative learning is Hebbian plasticity, where synapses that contribute to the firing of a post-synaptic neuron during encoding are strengthened and become capable of influencing the neuron's reactivation at recall.[56,57] Hebbian plasticity can involve synaptic weakening though, typically by LTD of non-relevant synapses (synapses whose activity did not match with that of the post-synaptic cell).[43,58] This process plays a minor role in encoding compared to that of Hebbian LTP, which is essential for the cell's reactivation. Our results fit better with anti-Hebbian plasticity, where synapses that contributed to the firing of a post-synaptic neuron are weakened, thus promoting future negative responses. Anti-Hebbian LTD has been described in detail in the cerebellum and is CaMKII-dependent.[30,31,45,46] In our work, synaptic weakening targets relevant synapses, and leads to a reduced response to the tone in M1. Such negative representations (stimulus responses that are below chance level) are brought about by negative plasticity and give rise to negative movement responses. As volume is a limited resource in the brain, negative representations may also be beneficial as an inexpensive way to increase storage capacity.

We identified a post-synaptic mechanism for the acquisition of negative responses by focusing on acquired responses. Identifying such a mechanism would have been more challenging in innate negative responses, as it would require determining if negative synaptic responses are below chance level. It is easier to determine that something disappears than that it is absent. That being said, given the prevalence of negative responses, it should be possible to identify innate or developmental negative representations. For example, Zeharia et al., 2012, found in M1 a topographic representation of a "negative homunculus"; areas whose activity was anti-correlated with movement, inlaid inversely to M1's typical (positive) homunculus. For example, cortical locations with positive responses to tongue movements exhibited negative responses to leg movements.[5]

M1's potential as a target for therapy of memory-related pathologies, such as PTSD, is promising but not yet realized. This is evident in the minor consideration (if any) that M1 received in recent influential reviews on fear circuitry and freezing.[16,24,25] This lack of acknowledgement may be due in part to the fact that learning is often associated with gaining positive rather than negative responses. For example, of the two back-to-back

papers of Gordon Shulman and colleagues,[1,2] that were instrumental in identifying the deactivation of the brain's default mode network,[4] the one devoted to positive responses is cited about 100 times more than the one devoted to negative ones (!). Another reason for overlooking M1 as a therapeutic target is that M1 is linked intuitively with movement, not its suppression, and thus may appear less relevant for freezing and threat responses.[59,60] Third, M1 is often viewed as an operative agent that executes movement and is not involved in emotional memories.[20] As these notions evolve, due to M1's accessible location for trans-cranial manipulations, it may represent a promising target for the treatment of pathologies in which emotional memories go awry.

Star Methods

RESOURCE AVAILABILITY

Lead contact—Further communication should be directed to the lead contact, Erez Geron (Erez.geron@nyulangone.org).

Materials availability—This study did not generate new reagents.

Data and code availability

- All data reported in this paper will be shared by the lead contact upon request.
- This paper does not report original code.
- Any additional information required to reanalyze the data reported in this paper is available from the lead contact upon request.

EXPERIMENTAL MODEL AND SUBJECT DETAILS

Animals—All experiments involving animals were in accordance with NIH guidelines and approved by the NYULMC IACUC. Male and female C57BL/6 mice at postnatal days (P) 30–50 were used for experiments. We did not detect a significant difference between freezing levels of male and female animals (% freezing to tone: females: 11.8 ± 5.8 (n = 34); males: 15.2 ± 6.2 % (n = 39); p = 0.33, unpaired t-test). Animals were group housed on a 12-hour light/dark cycle with light on at 8 AM. Animals had free access to food, water, and nesting material. Animals were of non-conditioned parents. All experiments were initiated during the light on period. Animals were randomly assigned to experimental groups.

METHOD DETAILS

Surgical procedures

Intracranial AAV injections of neonates: Sparse double labeling of PNs was achieved as described before series.[61] In short, pups at postnatal day 1–3 were anesthetized by hypothermia and a beveled micropipette was used (freehand) to penetrate the skin and skull and deliver 50–150 nL of the virus mix. M1 injection site was determined using the head's veins as reference points. We found it important to maintain high titers of the injected viruses and performed the following serial dilutions. For these one would have to have a dye stock solution (fast-green, Sigma Aldrich, F725; 6 % w/v). The Cre-harboring virus was first diluted in ACSF (1:700 to 1:1200, initial titer: 10^{13} VG/mL). This dilution was

then diluted in one-to-one with the dye solution. The Cre/dye mix was then diluted in the tdTomato-harboring virus at a ratio of 1:7 (7-fold excess of the tdTomato-harboring virus). Finally, the Cre/dye//tdTomato cocktail was mixed with the GCaMP-harboring virus at a 1:4 ratio (4-fold excess of the GCaMP virus). Therefore, the injected virus mix contained 80 % GCaMP-harboring virus, 17.5 % tdTomato-harboring virus, and ~2.5 % ACSF (containing the Cre-harboring virus and the fast-green dye). A fresh virus mix was prepared for each day used.

Intracranial AAV injections of P21 animals: Animals in experiments requiring dense labeling of ArchT-tdTomato, paAIP2-CyRFP were injected at P21–25. Animals were anesthetized with an intraperitoneal (IP) injection of ketamine (100 mg/kg) and xylazine (10 mg/kg). Eye ointment was applied. The mouse head was shaved and lidocaine (0.5–1 %) was applied on the shaved scalp. The skull surface was exposed with a midline incision. Then, a 0.5 mm hole was produced on the animal's skull at 0.3 mm anterior and 1.2 mm lateral to bregma. Subsequently, a beveled glass pipette was used to penetrate the brain using a micromanipulator (M3301 World Precision Instruments), at a 60-degree angle relative to the skull surface (550–750 μm in depth). Then, 50–100 nL of virus were delivered over ~10 minutes (Picospritzer III; 20 p.s.i., 20 ms, 0.2 Hz). For dense labeling of Cre-dependent ArchT-tdTomato or Cre-dependent paAIP2-CyRFP, the CaMKII::Cre virus was tittered to a final concentration of 10^{12} VG/ mL. The animal and the pipette were not moved for an additional 5–10 minutes. Subsequently, the temporary skull holder was gently removed, and the skin incision sutured. Animals were then placed on a heating pad until regaining mobility, and afterwards were returned to their home cage. Animals under this section, and in all other sections that involved KX anesthesia, were administered with Meloxicam (5 mg/kg; subcutaneously) once a day for 3 three days after surgery.

Mounting of a permanent skull-attached head holder: A day prior to experiments requiring head restart, mice underwent surgery to attach a head holder. Specifically, mice were anesthetized with an IP injection of ketamine and xylazine (100 and 10 mg/kg, respectively). The scalp was shaved and injected with lidocaine (0.5–1 %). Subsequently, the scalp was removed, and lidocaine was immersed over the exposed periosteum tissue. A few minutes later, the periosteum tissue was removed using a fine micro-blade. Using cyanoacrylate-based glue, two parallel metal bars were attached to the skull to serve as a head holder. A well was molded from dental acrylic cement around the bars.

Installing cranial windows: A craniotomy was performed above the caudal forelimb in M1[37] (AP: −0.5 ↔ +1 mm; DL: 1↔3 mm).[37] After removal of the skull, the exposed brain was kept wet with artificial cerebrospinal fluid and covered with a glass coverslip.

Behavioral studies

Fear conditioning

Training in a conditioning box: Mice were trained in a conditioning box equipped with a stainless-steel shocking grid connected to a precision feedback current-regulated shocker. This box was held within a sound-attenuating chamber (Coulbourn Instruments).

Behavior was recorded by low-light video camera. Stimuli (tone and shock) presentation was automated by using Actimetrics FreezeFrame software (Coulbourn Instruments).

Habituated to the box and tone (total of ten minutes with two tone presentations: 4 kHz, 75 dB, 20 s; intertrial interval (ITI): 3 minutes). For training, after 5 minutes in the box, the mice were subjected to the indicated training protocol. The parameters used were: tone: 4 kHz, 75 dB, 20 s; electric shock: 0.3 mA, 2 s; ITI: 90 s. For associative training, the tone and shock were co-terminating. For the unpaired group, the shock offset preceded the tone by 8 seconds. Animals were removed from the box 8–10 minutes after shock offset. The box was cleaned (EtOH then water) and dried between animals.

Recall test was performed in a different box, placed in a different room, and with a different context from the training box used during conditioning (non-shocking grids and different orientation marks). Mice were habituated to the box for 5.minutes and presented with the tone for 2 minutes. Five minutes after tone offset, the examined animal was returned to its home cage.

Fear conditioning under the microscope

Construction of the conditioning plate: Fear conditioning was performed using a simple, lab-built apparatus, constructed by attaching two sheets of aluminum foil to a non-conductive restraining plate (Figure S1A). The plate was connected to an isolated pulse stimulator (A-M systems M 2100), and the shock strength was measured directly from the sheets using an ammeter.

Habituation to handling, head restraint, and tone: Fear conditioning of head-restrained mice requires an attentive pre-training procedure. The mice were provided with wet food and habituated to handling for at least two weeks before the head-mount surgery. Before imaging, the mice habituated to restraint in the imaging apparatus. Habituation was conducted twice for 10 and 15 minutes, and included 2 tone presentations of a 4 kHz, 75dB, 20 s; 3 min ITI). Animals resisting restraint (release cutoff: vocalizing or struggling for more than 20 continuous seconds) were returned to their cage and tested again after more than 20 min.

Training and recall: The animals were placed on the conditioning plate and allowed to freely explore the imaging arena for at least 5 minutes (plate size: 15 × 35 cm). Ca^{2+} imaging started ~10 minutes after restraining. Stimuli parameters: tone: 4 kHz, 75 dB, 20 s; electric shock: 0.5 mA, 2 s; ITI: 90 s. The timing of the stimuli presentation was predetermined. For the unpaired group, the shock offset preceded the tone by 8 seconds. Imagining continued for 3–6 minutes after shock offset, and the animal was returned to its home cage subsequently. We trained the animal in a relatively short interval after surgery (acute imaging) to leverage the high optical access this approach provides.

For imaged recall tests, the animals were restrained and imaged for at least 2 minutes before tone presentations. The tone was presented for 30 s. Animals bearing double-labeled neurons were tested for recall twice, once for the dendrites and once for soma. The conditioning plate was cleaned with water and ethanol and dried before each time used.

Learning was assessed 24 h after training by measuring the freezing response to the auditory cue in a standard conditioning box. Here, animals were habituated to the box for 10 minutes before the tone was presented for 2 minutes (75dB). We chose not to test freezing in a box 4 h after training not to burden the animals and since freezing at early time points are lower than at a day after training (Figures S1B, C). It should be noted that in agreement with others [23], mice exhibited freezing already during training (e.g., the pairing + tone protocol), and that freezing at training correlated strongly with freezing at the 24 h recall test (Figure S1D), indicating a positive relation between early and late levels of learning.

Training under the microscope yielded low freezing levels compared to training in a box (Figures 1C, D). To test if freezing levels after training under the microscope could be manipulated. We compared standard conditioning parameters to quiet settings during recall (achieved by turning the fan of the conditioning box off). Quiet recall settings resulted in higher freezing levels (Figure S1E). In Figure 2, we used data from mice demonstrating strong learning under the microscope. We considered mice to be good learners if their performance fulfilled two criteria: freezing to the tone that exceeded the median (median freezing level was 8.65 % and the cutoff was set at 10%), and a two-fold increase in freezing upon tone presentation. Good learners were significantly distinct from bad learners: $\chi^2(1) = 57.947$, $p < .001$, Kruskal-Wallis test, n= 40 good and 48 bad learners. (See also Figure S1H)

Summary of animal exclusion criteria: We removed animals from the study in the following conditions: 1. Too big litters. In accordance with others,[62] we limited litter size to 4–5 pups per dam. 2. We excluded runts, and animals performing or subjected to barbering. 3. We excluded animals with bad recovery from surgery: loss of more than 10% of weight within a day after surgery, scruffy coat, apathy, and hunched posture. We estimate these constituted less than five percent of animals operated on. 3. We excluded animals that did not habituate to restraint: mice resisting restraint (cut off for release: struggle and/or vocalizing for more than 20 s), the animals were returned to their home cage. Animals resisting restraint in three tries were removed from the study (total of 3 animals). 4. We excluded animals that expressed high levels of basal anxiety, indicated by high freezing levels during the first visit to the imaging arena (> 20 % of the time). At this time, mice are very aroused and hardly stop moving and inspecting the stage, let alone freeze. We therefore consider freezing at this period as indicator of elevated anxiety and refrained from testing these animals.

Possible optimizations for training under the microscope: We used acute imaging, which facilitated spine imaging. However, this required a short interval between craniotomy and imaging (a day), most likely compromising freezing levels at recall. We recommend separating the head-holder surgery and the craniotomy by several days or using chronic imaging, where the interval between the craniotomy and imaging is greater than two weeks. These changes would allow a better time frame for recovery from the surgery and for habituation to restraint.

Optogenetic and chemogenetic manipulations: Optogenetics was used to inhibit neuronal activity with ArchT or to inhibit CaMKII activity using paAIP2. For experiments involving

ArchT-tdTomato, four days before training, the animals were anesthetized and their skull was exposed and thinned above M1, and mating sleeves (Thor labs; ADAL1) were installed over the thinned regions. The exposed area was sealed with acrylic glue and dental cement, which also secured the sleeves in place. Animals were then placed on a heating pad until regaining mobility, and afterwards were returned to their home cage. Before entry to the box, the mating sleeves were connected to an optical fiber (Thor labs; BFYL2LS01), which was connected to a fiber-coupled LED (Thor labs; M565F3; 565nm). The animals were conditioned in a box with the pairing + tone protocol, with light on during the second tone (Figure 1F'). Light power was adjusted to reach not more than 15mW/cm^2 on the tissue.

In all experiments requiring CaMKII inhibition, animals were conditioned under the microscope was described in the main text. Here, an optical fiber was positioned adjacent to the objective and the imaging area, so it could illuminate the imaged cells (light was delivered from fiber-coupled LEDs (Thor labs; blue: 470nm, M470F3, orange: M565F3; 565nm). The second illumination was delivered in the home cage. For experiments involving CaMKII inhibition without imaging (Figure 6H), the optical fiber was positioned, during training, directly above M1 (unilateral labeling). Light power was adjusted to reach approximately 15mW/cm^2 at the cortex.

We performed two types of experiments involving manipulation of PV INs activity. In the first, we verified that inhibiting PV INs increases the activity of adjacent PNs. Here, PV-Cre mice were injected with a virus carrying a CaMKII::GCaMP6s construct together with another virus harboring a Cre-dependent hM4D(Gi)-mCherry or a Cre-dependent tdTomato construct. Three weeks after virus injection, mounted with head-holder and a cranial window. The subsequent day, GCaMP signal was imaged before and after (20 min) administration of CNO (ip, 3 mg/kg). In a second experiment, to test the effect of M1 activation on freezing, PV-Cre mice were injected with a virus carrying a Cre-dependent hM4D(Gi)-mCherry or a Cre-dependent EGFP constructs. Three weeks after virus injection, animals were trained in a conditioning box without manipulation (the pairing + tone protocol). The subsequent day, 20 minutes before the start the recall test, the animals were administered IP with CNO (3 mg/kg). At training and recall, experimenters were blind to the virus injected.

Imaging: Imagining was conducted using Olympus FV1000, FV1000MPE, and a Bruker Ultima Investigator imaging systems equipped with a 25X/1.05 NA Olympus objectives. We used an IR filter cube BA685, filter cube for CH1/CH2 detectors FV-FGR. Barrier filter for CH1 (red): BA575–645; CH2 (green): BA495–540. Laser was supplied by Ti:Sapphire lasers (MaiTai DeepSee, Spectra Physics). Laser wavelength was tuned to 920 nm for all experiments but those involving the paAIP2 construct (in which we used 965 nm to prevent paAIP2 activation). Laser power was adjusted not to exceed 10mW/Cm^2. For dendritic imaging, a frame rate was of 2–4 Hz, and 3–6 Hz for somatic imaging.

QUANTIFICATION AND STATISTICAL ANALYSIS

Quantification of freezing—To quantify freezing behavior, the freeze threshold was determined by examining the motion index histogram obtained from the Actimetrics

FreezeFrame software. These histograms typically exhibit two prominent peaks: the first peak, commencing at 0, represents freezing behavior, while the second, signifies movement. Between these peaks, there is a distinct trough, following the manufacturer's guidelines, the freezing threshold is set to the value associated with the trough.

Image analysis

Ca^{2+} data extraction: Ca^{2+} activity was measured by fluorescence changes of the GCaMP6s indicator. The GCaMP channel time series was first registered. Subsequently, regions-of-interest (ROIs) were created manually over an averaged projection of the registered time series. The registered image was inspected qualitatively to detect artifacts resulting from movements in the z or xy axes or from bleaching of the GCaMP signal. Time series with movements that precluded analysis for more than 10 % of the time were not included in the study (2 animals).

Excluding periods of activity from the calculation of the fluorescence level at rest (F_0), was especially important for assessing the activity of INs that often had persistent bouts of activity (for example, see Figure 2C). To not including periods of activity in the calculation of F_0, we first used the 20^{th} percentile to generate an initial ΔF/F trace. We then estimated that periods with activity above 20 % ΔF/F are likely periods of activity and that periods below −10% are times of movement artifacts. We then excluded these periods and determined F_0 as the 20th percentile of the remaining time. To control photobleaching effects, in cases where there was a reduction in fluorescence (at rest) that exceeded 5%, we used a moving average to determine F_0. In such a case, F_0 was calculated as the 20^{th} percentile of the raw signal within a window of 60 s. If a change in the signal resulted from a movement in z, a moving average was applied from the shift in z.

Dendritic spikes were defined as fluorescence elevation of 3 SDs above the baseline of the ΔF/F trace. F0 and the SD of the ΔF/F trace were determined individually for each branch. Spikes occurring within a time window of 1 s from other spikes were considered overlapping and were combined. For display of traces, ΔF/F values below −0.05 % were zeroed. In *Thy1.:*GCaMP6s animals, to minimize overrepresentation bias derived from multiple dendritic branches that likely originated from individual cells, branches displaying very similar activity patterns were combined ($r > 0.9$). In Figure 5A, median dendritic activity was calculated for the most active dendrite from each cell tested (n= 9 cells).

Analysis of spine Ca^{2+} activity—For the measurement of spine Ca^{2+} activity, time series were first registered. A median projection was created from the registered sequence and binarized. For each spine, an ROI encompassing its entire circumference was created manually. Subsequently, an ROI was created for the dendritic shaft such that it would not include any of its spines. We then extracted the raw dendritic spine activity and used this to calculate and remove the dendritic contribution to the spine activity [63]. F_0 was determined as the mode of the raw Ca^{2+} fluorescence. Using robust regression we regressed the spine $\Delta F/F_0$ against the shaft $\Delta F/F_0$ ($\Delta F/F_{0\_dendrite}$) and found the slope coefficient of the linear fit. Next, we multiplied $\Delta F/F_{0\_dendrite}$ by the slope coefficient and subtracted this scaled version of $\Delta F/F_{0\_dendrite}$ from the spine signal.

Quantifying a response—Responses to the tone were calculated by comparing the time of tone presentation to an equal period before it. Response values were achieved using the formula: $(\sum\Delta F/F_{tone} - \sum\Delta F/F_{before}) / (\sum\Delta F/F_{tone} + \sum\Delta F/F_{before})$. Response value of zero indicates no activity surpassing the activity threshold (3 SDs above the baseline) before or during the tone.

Clustering spines by activity at training—To cluster spines by activity, we first converted spines' dF/F traces into cumulative distribution functions (CDF; range 0–1), which allowed for distinguishing between spine traces with consistent activity (relatively consistent slope) and traces with activity during specific epochs (fluctuating slope). With these data, we determined the optimal number of non-negative matrix factorization (NMF) ranks by finding the elbow of matrix reconstruction error plotted against the rank number (k). The elbow was determined as the value of k for which the plot ($f(k)$) was the greatest distance from a straight line extending from $f(1)$ to $f(K)$, with $f(K)$ being the local minimum of the plot. We then performed NMF to generate rank-k matrices W and H. Cluster membership was assigned to observations (spines) based on the column containing their maximum value.

Spine size analysis—Analysis of spine size cannot rely on raw fluorescence values as these may vary between time points if factors such as laser power and PMT settings differ. Even if these are kept constant, changes in the preparation's quality (e.g., transparency) may yield differences in fluorescence values that do not reflect differences in size. Therefore, comparisons of spine size across time require normalization, typically performed by dividing the fluorescent readout of the spine by that of the dendritic shaft (Figures S6A–C).[27] To do so, we generated an ROI for each spine at its largest focal plane and a cognate shaft ROI. Subsequently, a background measurement was made for each spine and shaft pair and subtracted from them. Spine size was defined as the ratio of the spine to shaft measurements: (Mean spine fluorescence − background)/ (Mean shaft fluorescence − background). The change in spine size was calculated as follows: ((Spine size at T_1 or T_8)− (Spine size at T_0))/ (Spine size at T_0), and presented as percent change (Figure S6B).

Imagining for spine size assessment were conducted with a pixel size smaller than 0.3 μm. To minimize artifacts of pixel saturation, undersampling, and bleed-through from the GCaMP channel, 3 measurements were collected for each time point (data with saturated pixels were not analyzed). Measurements at different time points were of identical pixel size and z-step. Spines were defined as a protrusion with a head to neck ratio diameter above 1.2:1, and ratio of head length to neck length below 3:1.[27, 28 28 28 2828] Spine elimination is indicated as −100%. We found no spine formation over 1 h and 0.9 % formation over 8 h (2 spines). Analyses of spine size and activity were done blind of each other.

Analysis of body movements during head restraint—For the acquisition of gross body movement at recall in head-restraint animals, we imaged the animals' body using an infra-red camera (Basler aca1300–60gmnir) equipped with a Fujinon lens (1:1.3/2.7–13.5mm). Body and brain imaging were triggered at every frame to ensure synchrony. The resultant images of the body was binarize and the centroid of the largest object within a frame was determined using the vision.CornerDetector and vision.PointTracker functions

(MATLAB). Subsequently, the displacement of the centroid in x and y was derived, and overall displacement calculated (Pythagorean equation). Displacement was calculated in pixels.

Statistical analysis—We used t-test to compare two groups and one-way ANOVA (Fisher's LSD test) to compare more than two groups. All t-tests were conducted as two-tailed tests. We considered P values above 0.05 as not significant. Data are presented as average ± s.e.m.

Supplementary Material

Refer to Web version on PubMed Central for supplementary material.

Acknowledgments:

We thank B. Rudy and members of his lab for fruitful discussions and support. We also thank W. Gan and members of his lab. We thank O. Issler and R. Machold for comments on the manuscript, and D. Schiller. This work was supported by the National Institutes of Health grant: R01NS110079 to B. Rudy.

References

1. Shulman GL, Corbetta M, Buckner RL, Fiez JA, Miezin FM, Raichle ME, and Petersen SE (1997). Common Blood Flow Changes across Visual Tasks: I. Increases in Subcortical Structures and Cerebellum but Not in Nonvisual Cortex. J Cogn Neurosci 9, 624–647. 10.1162/jocn.1997.9.5.624. [PubMed: 23965121]
2. Shulman GL, Fiez JA, Corbetta M, Buckner RL, Miezin FM, Raichle ME, and Petersen SE (1997). Common Blood Flow Changes across Visual Tasks: II. Decreases in Cerebral Cortex. J Cogn Neurosci 9, 648–663. 10.1162/jocn.1997.9.5.648. [PubMed: 23965122]
3. Wade AR (2002). The negative BOLD signal unmasked. Neuron 36, 993–995. 10.1016/s0896-6273(02)01138-8. [PubMed: 12495615]
4. Buckner RL, and DiNicola LM (2019). The brain's default network: updated anatomy, physiology and evolving insights. Nat Rev Neurosci 20, 593–608. 10.1038/s41583-019-0212-7. [PubMed: 31492945]
5. Zeharia N, Hertz U, Flash T, and Amedi A (2012). Negative blood oxygenation level dependent homunculus and somatotopic information in primary motor cortex and supplementary motor area. Proc Natl Acad Sci U S A 109, 18565–18570. 10.1073/pnas.1119125109. [PubMed: 23086164]
6. Frith CD, Friston KJ, Liddle PF, and Frackowiak RS (1991). A PET study of word finding. Neuropsychologia 29, 1137–1148. 10.1016/0028-3932(91)90029-8. [PubMed: 1791928]
7. Huth AG, de Heer WA, Griffiths TL, Theunissen FE, and Gallant JL (2016). Natural speech reveals the semantic maps that tile human cerebral cortex. Nature 532, 453–458. 10.1038/nature17637. [PubMed: 27121839]
8. Rasser PE, Johnston P, Lagopoulos J, Ward PB, Schall U, Thienel R, Bender S, Toga AW, and Thompson PM (2005). Functional MRI BOLD response to Tower of London performance of first-episode schizophrenia patients using cortical pattern matching. Neuroimage 26, 941–951. 10.1016/j.neuroimage.2004.11.054. [PubMed: 15955504]
9. Hasenkamp W, James GA, Boshoven W, and Duncan E (2011). Altered engagement of attention and default networks during target detection in schizophrenia. Schizophr Res 125, 169–173. 10.1016/j.schres.2010.08.041. [PubMed: 20869846]
10. Shackman AJ, Fox AS, Oler JA, Shelton SE, Davidson RJ, and Kalin NH (2013). Neural mechanisms underlying heterogeneity in the presentation of anxious temperament. Proc Natl Acad Sci U S A 110, 6145–6150. 10.1073/pnas.1214364110. [PubMed: 23538303]
11. Holschneider DP, Yang J, Sadler TR, Nguyen PT, Givrad TK, and Maarek JM (2006). Mapping cerebral blood flow changes during auditory-cued conditioned fear in the nontethered,

nonrestrained rat. Neuroimage 29, 1344–1358. 10.1016/j.neuroimage.2005.08.038. [PubMed: 16216535]

12. Butler T, Pan H, Tuescher O, Engelien A, Goldstein M, Epstein J, Weisholtz D, Root JC, Protopopescu X, Cunningham-Bussel AC, et al. (2007). Human fear-related motor neurocircuitry. Neuroscience 150, 1–7. 10.1016/j.neuroscience.2007.09.048. [PubMed: 17980493]
13. Xu Z, Adler A, Li H, Perez-Cuesta LM, Lai B, Li W, and Gan WB (2019). Fear conditioning and extinction induce opposing changes in dendritic spine remodeling and somatic activity of layer 5 pyramidal neurons in the mouse motor cortex. Sci Rep 9, 4619. 10.1038/s41598-019-40549-y. [PubMed: 30874589]
14. Quirk GJ, Armony JL, and LeDoux JE (1997). Fear conditioning enhances different temporal components of tone-evoked spike trains in auditory cortex and lateral amygdala. Neuron 19, 613–624. 10.1016/s0896-6273(00)80375-x. [PubMed: 9331352]
15. Watson TC, Cerminara NL, Lumb BM, and Apps R (2016). Neural Correlates of Fear in the Periaqueductal Gray. J Neurosci 36, 12707–12719. 10.1523/JNEUROSCI.1100-16.2016. [PubMed: 27974618]
16. Izquierdo I, Furini CR, and Myskiw JC (2016). Fear Memory. Physiol Rev 96, 695–750. 10.1152/physrev.00018.2015. [PubMed: 26983799]
17. Yang Y, Liu DQ, Huang W, Deng J, Sun Y, Zuo Y, and Poo MM (2016). Selective synaptic remodeling of amygdalocortical connections associated with fear memory. Nat Neurosci 19, 1348–1355. 10.1038/nn.4370. [PubMed: 27595384]
18. Omrani M, Kaufman MT, Hatsopoulos NG, and Cheney PD (2017). Perspectives on classical controversies about the motor cortex. J Neurophysiol 118, 1828–1848. 10.1152/jn.00795.2016. [PubMed: 28615340]
19. Peters AJ, Liu H, and Komiyama T (2017). Learning in the Rodent Motor Cortex. Annu Rev Neurosci 40, 77–97. 10.1146/annurev-neuro-072116-031407. [PubMed: 28375768]
20. Ebbesen CL, Insanally MN, Kopec CD, Murakami M, Saiki A, and Erlich JC (2018). More than Just a “Motor”: Recent Surprises from the Frontal Cortex. J Neurosci 38, 9402–9413. 10.1523/JNEUROSCI.1671-18.2018. [PubMed: 30381432]
21. Northoff G, Walter M, Schulte RF, Beck J, Dydak U, Henning A, Boeker H, Grimm S, and Boesiger P (2007). GABA concentrations in the human anterior cingulate cortex predict negative BOLD responses in fMRI. Nat Neurosci 10, 1515–1517. 10.1038/nn2001. [PubMed: 17982452]
22. Lauritzen M, Mathiesen C, Schaefer K, and Thomsen KJ (2012). Neuronal inhibition and excitation, and the dichotomic control of brain hemodynamic and oxygen responses. Neuroimage 62, 1040–1050. 10.1016/j.neuroimage.2012.01.040. [PubMed: 22261372]
23. Fanselow MS (1980). Conditioned and unconditional components of post-shock freezing. Pavlov J Biol Sci 15, 177–182. 10.1007/BF03001163. [PubMed: 7208128]
24. Roelofs K (2017). Freeze for action: neurobiological mechanisms in animal and human freezing. Philos Trans R Soc Lond B Biol Sci 372. 10.1098/rstb.2016.0206.
25. Roelofs K, and Dayan P (2022). Freezing revisited: coordinated autonomic and central optimization of threat coping. Nat Rev Neurosci 23, 568–580. 10.1038/s41583-022-00608-2. [PubMed: 35760906]
26. Bartol TM, Bromer C, Kinney J, Chirillo MA, Bourne JN, Harris KM, and Sejnowski TJ (2015). Nanoconnectomic upper bound on the variability of synaptic plasticity. Elife 4, e10778. 10.7554/eLife.10778. [PubMed: 26618907]
27. Zhang Y, Cudmore RH, Lin DT, Linden DJ, and Huganir RL (2015). Visualization of NMDA receptor-dependent AMPA receptor synaptic plasticity in vivo. Nat Neurosci 18, 402–407. 10.1038/nn.3936. [PubMed: 25643295]
28. Bai Y, Li M, Zhou Y, Ma L, Qiao Q, Hu W, Li W, Wills ZP, and Gan WB (2017). Abnormal dendritic calcium activity and synaptic depotentiation occur early in a mouse model of Alzheimer’s disease. Mol Neurodegener 12, 86. 10.1186/s13024-017-0228-2. [PubMed: 29137651]
29. Matsuzaki M, Honkura N, Ellis-Davies GC, and Kasai H (2004). Structural basis of long-term potentiation in single dendritic spines. Nature 429, 761–766. 10.1038/nature02617. [PubMed: 15190253]

30. Feldman DE (2012). The spike-timing dependence of plasticity. Neuron 75, 556–571. 10.1016/j.neuron.2012.08.001. [PubMed: 22920249]
31. Ito M (2001). Cerebellar long-term depression: characterization, signal transduction, and functional roles. Physiol Rev 81, 1143–1195. 10.1152/physrev.2001.81.3.1143. [PubMed: 11427694]
32. Bell CC, Han VZ, Sugawara Y, and Grant K (1997). Synaptic plasticity in a cerebellum-like structure depends on temporal order. Nature 387, 278–281. 10.1038/387278a0. [PubMed: 9153391]
33. Aime M, Augusto E, Kouskoff V, Campelo T, Martin C, Humeau Y, Chenouard N, and Gambino F (2020). The integration of Gaussian noise by long-range amygdala inputs in frontal circuit promotes fear learning in mice. Elife 9. 10.7554/eLife.62594.
34. d'Aquin S, Szonyi A, Mahn M, Krabbe S, Grundemann J, and Luthi A (2022). Compartmentalized dendritic plasticity during associative learning. Science 376, eabf7052. 10.1126/science.abf7052. [PubMed: 35420958]
35. Maren S (2014). Nature and causes of the immediate extinction deficit: a brief review. Neurobiol Learn Mem 113, 19–24. 10.1016/j.nlm.2013.10.012. [PubMed: 24176924]
36. Kim SC, Jo YS, Kim IH, Kim H, and Choi JS (2010). Lack of medial prefrontal cortex activation underlies the immediate extinction deficit. J Neurosci 30, 832–837. 10.1523/JNEUROSCI.4145-09.2010. [PubMed: 20089891]
37. Tennant KA, Adkins DL, Donlan NA, Asay AL, Thomas N, Kleim JA, and Jones TA (2011). The organization of the forelimb representation of the C57BL/6 mouse motor cortex as defined by intracortical microstimulation and cytoarchitecture. Cereb Cortex 21, 865–876. 10.1093/cercor/bhq159. [PubMed: 20739477]
38. Cichon J, Magrane J, Shtridler E, Chen C, Sun L, Yang G, and Gan WB (2020). Imaging neuronal activity in the central and peripheral nervous systems using new Thy1.2-GCaMP6 transgenic mouse lines. J Neurosci Methods 334, 108535. 10.1016/j.jneumeth.2019.108535. [PubMed: 31972184]
39. Tremblay R, Lee S, and Rudy B (2016). GABAergic Interneurons in the Neocortex: From Cellular Properties to Circuits. Neuron 91, 260–292. 10.1016/j.neuron.2016.06.033. [PubMed: 27477017]
40. Schuman B, Machold RP, Hashikawa Y, Fuzik J, Fishell GJ, and Rudy B (2019). Four Unique Interneuron Populations Reside in Neocortical Layer 1. J Neurosci 39, 125–139. 10.1523/JNEUROSCI.1613-18.2018. [PubMed: 30413647]
41. Borgomaneri S, Vitale F, Gazzola V, and Avenanti A (2015). Seeing fearful body language rapidly freezes the observer's motor cortex. Cortex 65, 232–245. 10.1016/j.cortex.2015.01.014. [PubMed: 25835523]
42. Golding NL, Staff NP, and Spruston N (2002). Dendritic spikes as a mechanism for cooperative long-term potentiation. Nature 418, 326–331. 10.1038/nature00854. [PubMed: 12124625]
43. Sweatt JD (2016). Neural plasticity and behavior - sixty years of conceptual advances. J Neurochem 139 Suppl 2, 179–199. 10.1111/jnc.13580.
44. Sjostrom PJ, Rancz EA, Roth A, and Hausser M (2008). Dendritic excitability and synaptic plasticity. Physiol Rev 88, 769–840. 10.1152/physrev.00016.2007. [PubMed: 18391179]
45. Hansel C, de Jeu M, Belmeguenai A, Houtman SH, Buitendijk GH, Andreev D, De Zeeuw CI, and Elgersma Y (2006). alphaCaMKII Is essential for cerebellar LTD and motor learning. Neuron 51, 835–843. 10.1016/j.neuron.2006.08.013. [PubMed: 16982427]
46. Harvey-Girard E, Lewis J, and Maler L (2010). Burst-induced anti-Hebbian depression acts through short-term synaptic dynamics to cancel redundant sensory signals. J Neurosci 30, 6152–6169. 10.1523/JNEUROSCI.0303-10.2010. [PubMed: 20427673]
47. Bayer KU, and Schulman H (2019). CaM Kinase: Still Inspiring at 40. Neuron 103, 380–394. 10.1016/j.neuron.2019.05.033. [PubMed: 31394063]
48. Murakoshi H, Shin ME, Parra-Bueno P, Szatmari EM, Shibata ACE, and Yasuda R (2017). Kinetics of Endogenous CaMKII Required for Synaptic Plasticity Revealed by Optogenetic Kinase Inhibitor. Neuron 94, 690. 10.1016/j.neuron.2017.04.027. [PubMed: 28472663]
49. Roediger HL 3rd, and Butler AC (2011). The critical role of retrieval practice in longterm retention. Trends Cogn Sci 15, 20–27. 10.1016/j.tics.2010.09.003. [PubMed: 20951630]

50. Cohen N, Pell L, Edelson MG, Ben-Yakov A, Pine A, and Dudai Y (2015). Peri-encoding predictors of memory encoding and consolidation. Neurosci Biobehav Rev 50, 128–142. 10.1016/j.neubiorev.2014.11.002. [PubMed: 25446944]
51. Antony JW, Ferreira CS, Norman KA, and Wimber M (2017). Retrieval as a Fast Route to Memory Consolidation. Trends Cogn Sci 21, 573–576. 10.1016/j.tics.2017.05.001. [PubMed: 28583416]
52. Cummings KA, Bayshtok S, Dong TN, Kenny PJ, and Clem RL (2022). Control of fear by discrete prefrontal GABAergic populations encoding valence-specific information. Neuron 110, 3036–3052 e3035. 10.1016/j.neuron.2022.07.004. [PubMed: 35944526]
53. Courtin J, Chaudun F, Rozeske RR, Karalis N, Gonzalez-Campo C, Wurtz H, Abdi A, Baufreton J, Bienvenu TC, and Herry C (2014). Prefrontal parvalbumin interneurons shape neuronal activity to drive fear expression. Nature 505, 92–96. 10.1038/nature12755. [PubMed: 24256726]
54. Diaz-Mataix L, Piper WT, Schiff HC, Roberts CH, Campese VD, Sears RM, and LeDoux JE (2017). Characterization of the amplificatory effect of norepinephrine in the acquisition of Pavlovian threat associations. Learn Mem 24, 432–439. 10.1101/lm.044412.116. [PubMed: 28814469]
55. Labarrera C, Deitcher Y, Dudai A, Weiner B, Kaduri Amichai A, Zylbermann N, and London M (2018). Adrenergic Modulation Regulates the Dendritic Excitability of Layer 5 Pyramidal Neurons In Vivo. Cell Rep 23, 1034–1044. 10.1016/j.celrep.2018.03.103. [PubMed: 29694883]
56. Poo MM, Pignatelli M, Ryan TJ, Tonegawa S, Bonhoeffer T, Martin KC, Rudenko A, Tsai LH, Tsien RW, Fishell G, et al. (2016). What is memory? The present state of the engram. BMC Biol 14, 40. 10.1186/s12915-016-0261-6. [PubMed: 27197636]
57. Josselyn SA, and Tonegawa S (2020). Memory engrams: Recalling the past and imagining the future. Science 367. 10.1126/science.aaw4325.
58. Connor SA, and Wang YT (2016). A Place at the Table: LTD as a Mediator of Memory Genesis. Neuroscientist 22, 359–371. 10.1177/1073858415588498. [PubMed: 25993993]
59. Ebbesen CL, and Brecht M (2017). Motor cortex - to act or not to act? Nat Rev Neurosci 18, 694–705. 10.1038/nrn.2017.119. [PubMed: 29042690]
60. Noorani I, and Carpenter RH (2017). Not moving: the fundamental but neglected motor function. Philos Trans R Soc Lond B Biol Sci 372. 10.1098/rstb.2016.0190.
61. Geron E (2022). Glocal dendritic spikes: variation in branch activity during dendritic spiking indicates multiple functional units in the pyramidal neuron apical tuft. bioRxiv.
62. Cowan CSM, and Richardson R (2018). A Brief Guide to Studying Fear in Developing Rodents: Important Considerations and Common Pitfalls. Curr Protoc Neurosci 83, e44. 10.1002/cpns.44. [PubMed: 30040208]
63. Chen TW, Wardill TJ, Sun Y, Pulver SR, Renninger SL, Baohan A, Schreiter ER, Kerr RA, Orger MB, Jayaraman V, et al. (2013). Ultrasensitive fluorescent proteins for imaging neuronal activity. Nature 499, 295–300. 10.1038/nature12354. [PubMed: 23868258]

- During fear recall, the motor cortex displays negative neuronal responses
- These negative responses do not result from an overt increase in inhibition
- Dendritic spines active during fear conditioning undergo weakening
- This spine weakening supports negative responses and freezing

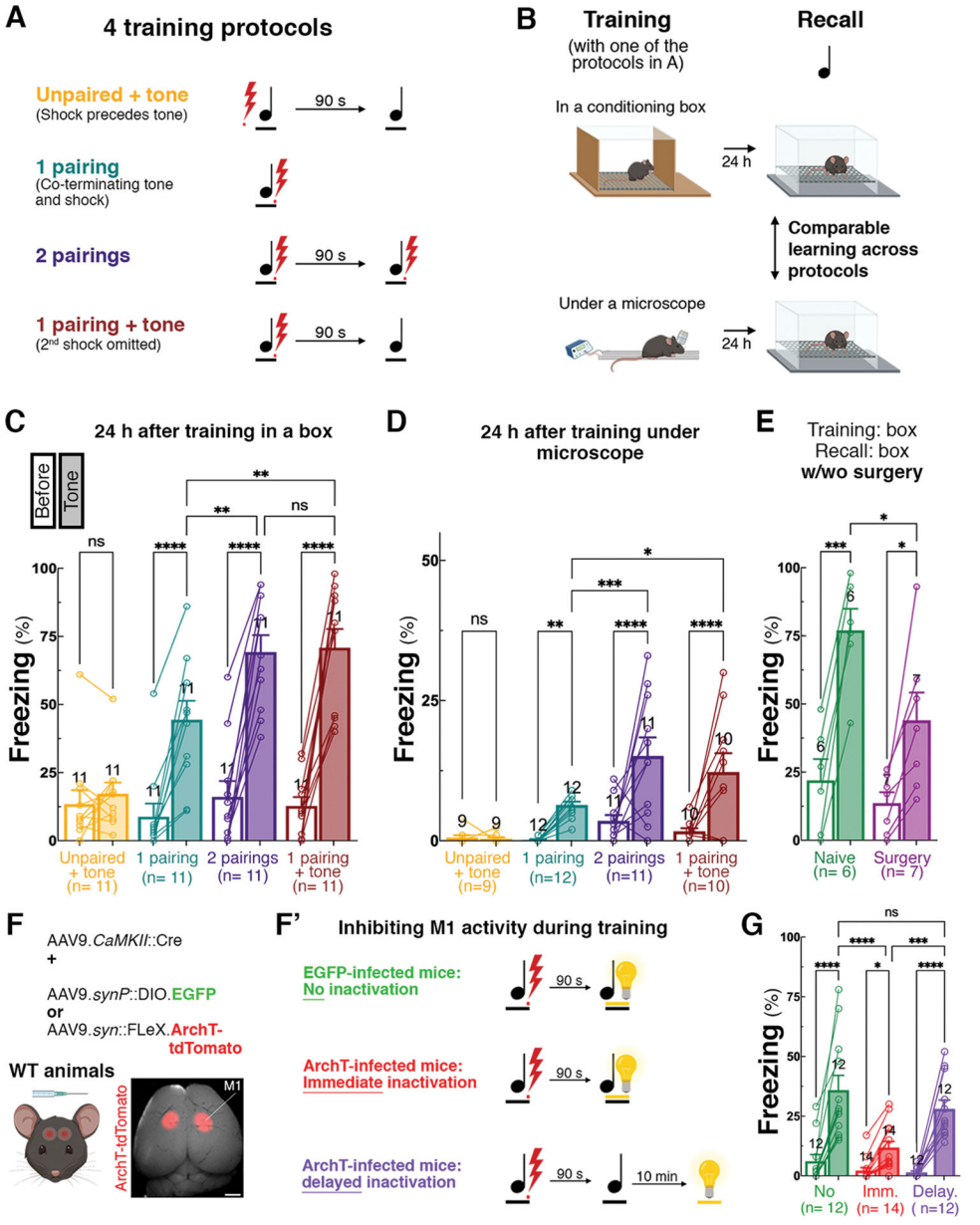

Figure 1. Fear learning under the microscope and a in box and its dependence on M1

(A)Training protocols used. The unpaired + tone protocol is a non-associative control procedure where the shock precedes the tone by 8 s. In the other associative protocols, the tone and shock were co-terminating.

(B-D) Mice were trained with one of the indicated protocols in a conditioning box or under a two-photon microscope, and freezing levels were tested in a box 24 h later (B). Freezing after training under a microscope was lower than after training in a box. However, in both settings, learning was evident only after associative training, and training with two pairings or with a pairing + tone yielded more freezing than with a single pairing. Filled bars indicate the portion of time spent freezing during the tone, and open bars indicate it during an equal period before. (*p = 0.022; **p= 0.0087; ***p< 0.0008; ****p< 0.0001; One-way ANOVA; Fisher's LSD test; n = 9–12 animals per group.

(E) Naïve mice and mice that underwent surgery were trained in a box and tested for recall in a box 24 h later. While both animal groups exhibited learning, mice in the surgery group exhibited less freezing to the tone. (*p= 0.0432; ***p< 0.0005; One-way ANOVA; Fisher's LSD test; n = 6 & 7 animals per group).

(F-G) Animals were injected with AAVs to express the neuronal silencer ArchT-tdTomato or EGFP in pyramidal neurons of M1 (F). Training ensued three weeks later (F'). Only animals whose M1 was inactivated during training displayed reduced freezing at a 24 h recall test (G). (****p<0.0001; ***p= 0.0007; *p= 0.023; One-way ANOVA; Fisher's LSD test; n= 12–14 animals per group). The scale bar in F represents 1 mm.

See also Figure S1 and Video S1.

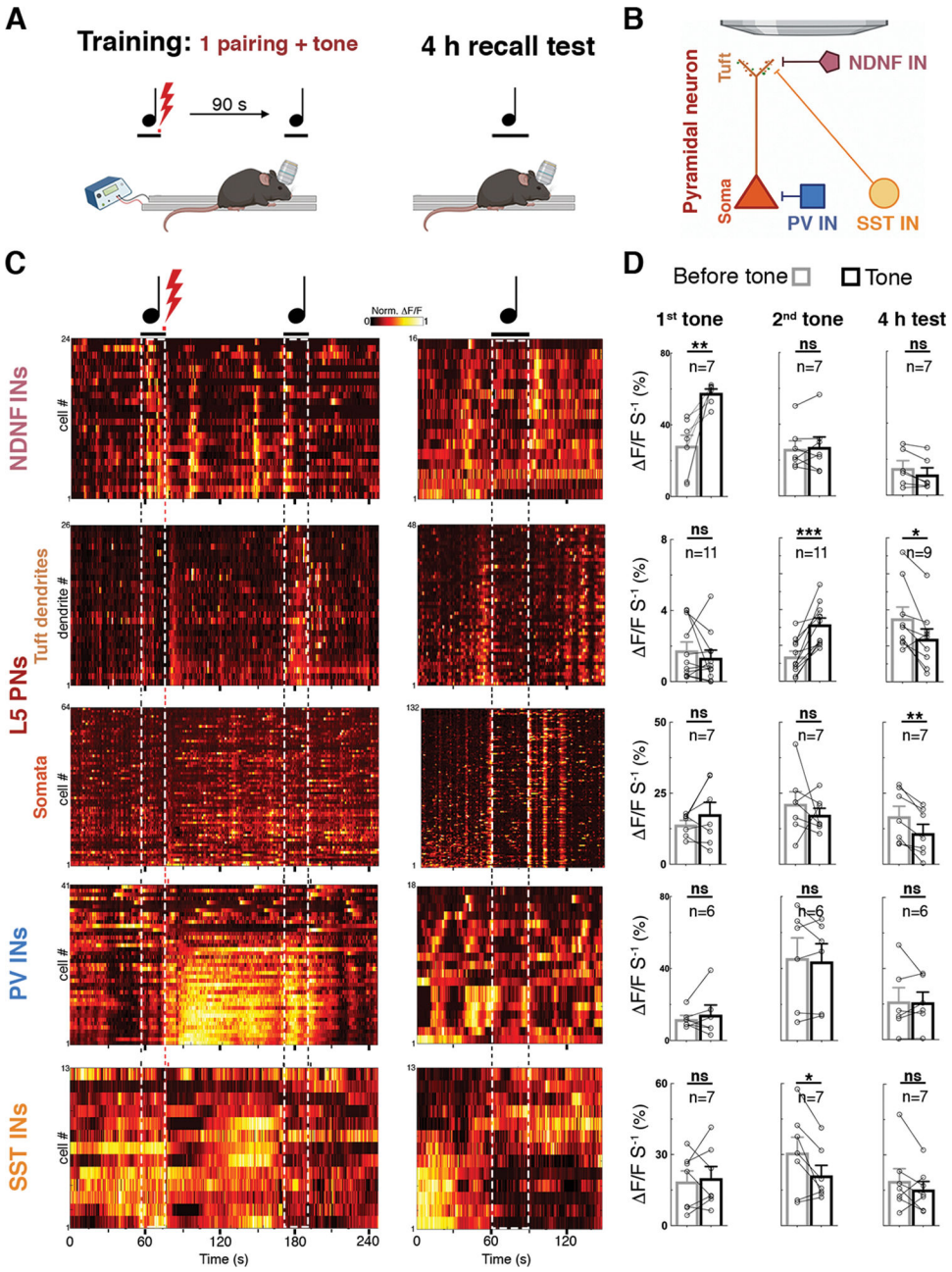

Figure 2. M1 L5 PNs develop negative tone responses without concomitant positive responses from INs that inhibit them

(A, B) Mice were imaged during training with the pairing + tone protocol and at a 4 h recall test, and Ca^{2+} activities in M1 were measured from the indicated cell types or compartments.

(C, D) Representative example heat maps and summary of Ca^{2+} activity. Heat maps depict all cells imaged in a single animal. Activity of each cell in the heat maps was normalized by the maximal activity value of that cell during the depicted period. The number of cells is indicated on the left of each heat map. Cells were sorted by activity during the shock (training; most active at the bottom) and baseline (recall). Each data pair in D represents

the averaged activity of all cells of a single animal. *p= 0.0409; **p= 0.0064; ***p= 0.002; paired t-test; n= 6–11 animals per group.
See also Figures S2, S4 and Videos S2, S3, S5.

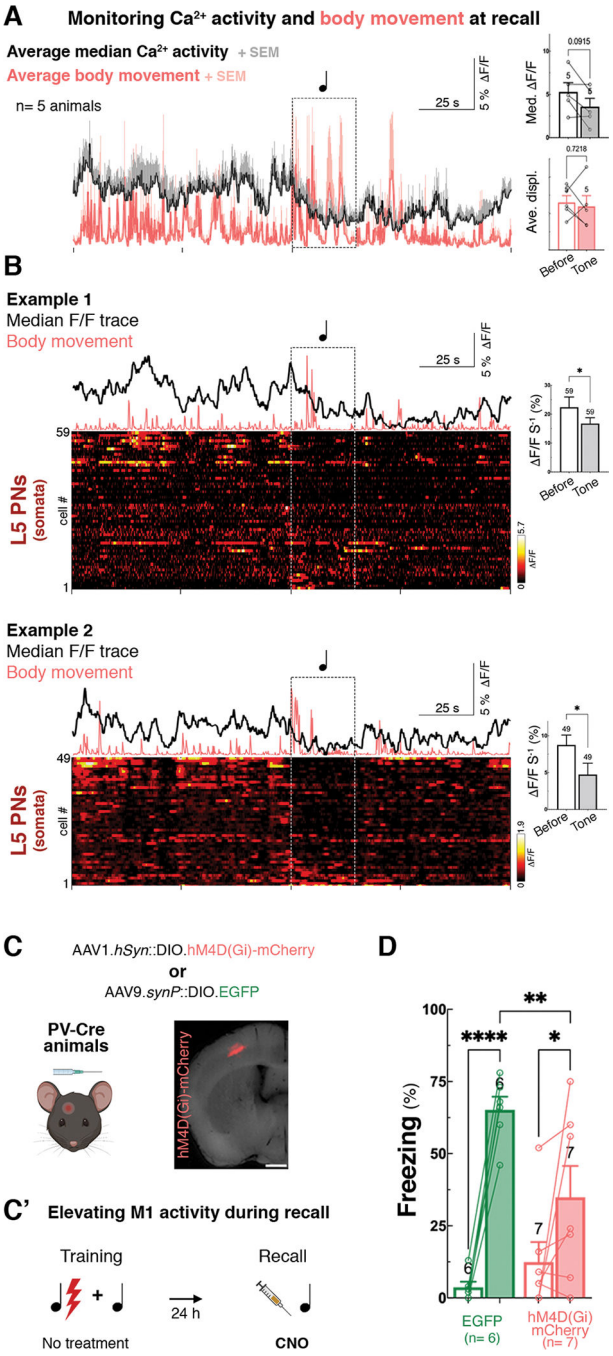

Figure 3. Negative responses in M1 support freezing

(A, B) Somatic activity of L5 PNs and simultaneous body movements during a recall test. In panel A, the ΔF/F activity and body displacement traces (black and pink, respectively) are presented for five animals. Quantification per animal is on the right. Panel B depicts two examples where Ca2+ is reduced without an apparent reduction in motion. Heat maps are sorted by response to the tone (negative at the top; (*p> 0.04; paired t-test n= 59 & 49). (C-D) PV-Cre animals were injected in M1 with AAVs harboring a Cre-dependent EGFP or a hM4D(Gi)-mCherry construct. Three weeks after injection, mice were trained

with the pairing + tone protocol without manipulation. A day after training, the mice were administered with CNO (3 mg/kg; IP). The recall test commenced 20 minutes afterward. (****p< 0.0001; **p= 0.0082; *p= 0.035; One-way ANOVA; Fisher's LSD test; n= 6–7 animals per group).

Scale bar in C represents 1 mm.

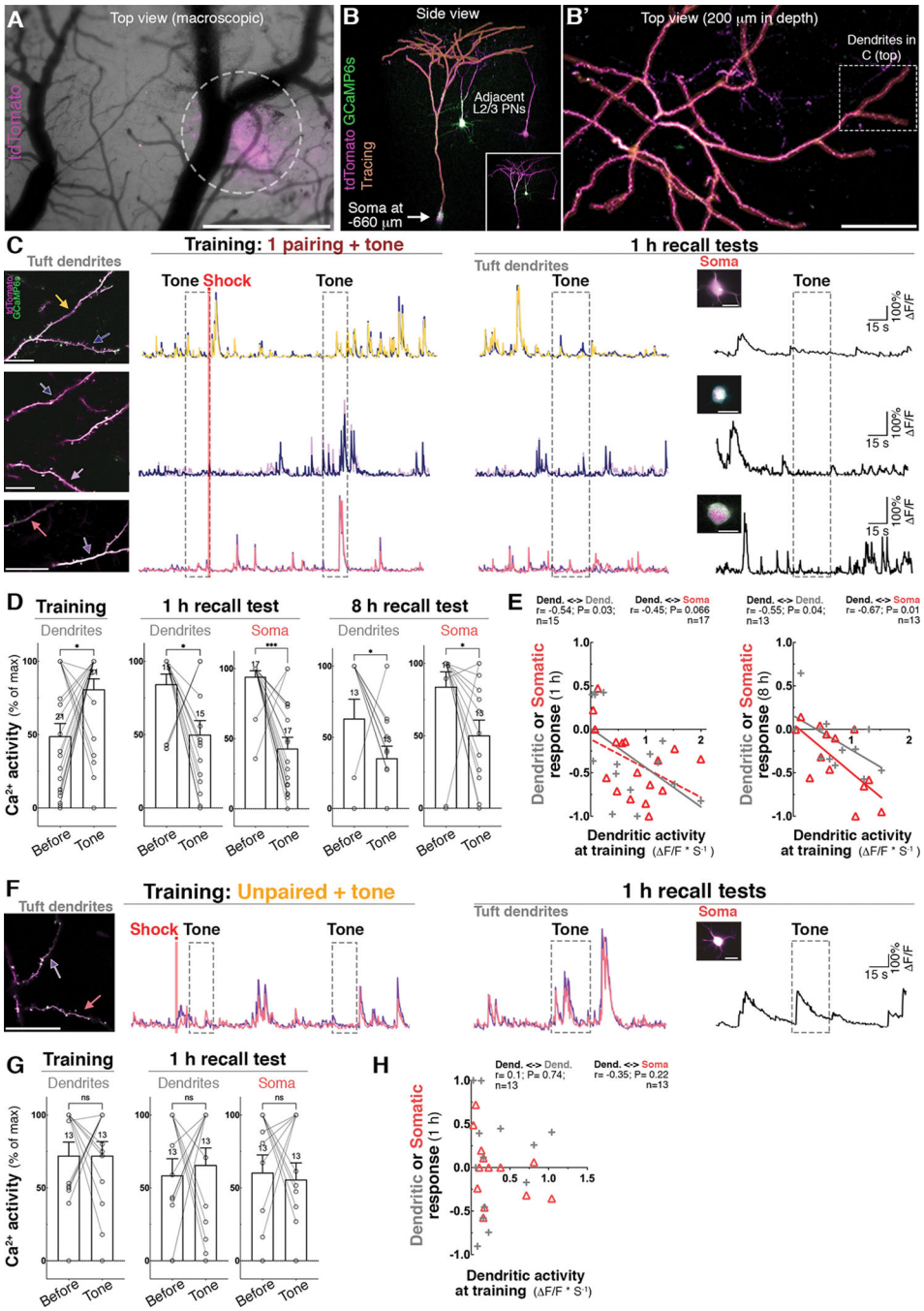

Figure 4. Emergence of negative tone responses of L5 PNs during associative learning

(A-B') Sparse labeling for visualizing activity in structurally defined neurons, dendrites, and spines. Top view of a cortical area of ~6 mm^2 bearing a single labeled tuft (circled) (**A**). Side and top view an L5 PN and adjacent L2/3 PNs (B, B'). The image was reconstructed from consecutive optical z-sections. The L5 PN is traced in orange. Inset in B exhibits the dendrite untraced. The boxed area in B' corresponds with the dendrites in panel C (top). A high green signal indicates high Ca^{2+} activity during the z-sections' imaging.

(C, D) Three example ΔF/F traces and summary of dendritic and somatic responses during associative training (with the pairing + tone protocol) and 1 and 8 h recall tests. Traces correspond with dendrites marked with matching-color arrows. Traces are scaled for each cell. *p= 0.048; ***p= 0.0004; n= 13–21 pairs; paired t-test. (E) Apical dendrites were first imaged during training. These dendrites and their soma were imaged during 1 and 8 h recall tests. Pearson's correlation: n= 15 & 17 pairs (1 h); 13 pairs (8 h).
(G-H) Dendritic and somatic Ca^{2+} activities during non-associative training (unpaired + tone) and 1h recall tests. Analyses are like those shown in panels C-E. Paired t-test.
Scale bars represent 1 mm in A, 100 μm in B', and 20 μm in C and F.
See also Figures S2–S4 and Videos S4, S5.

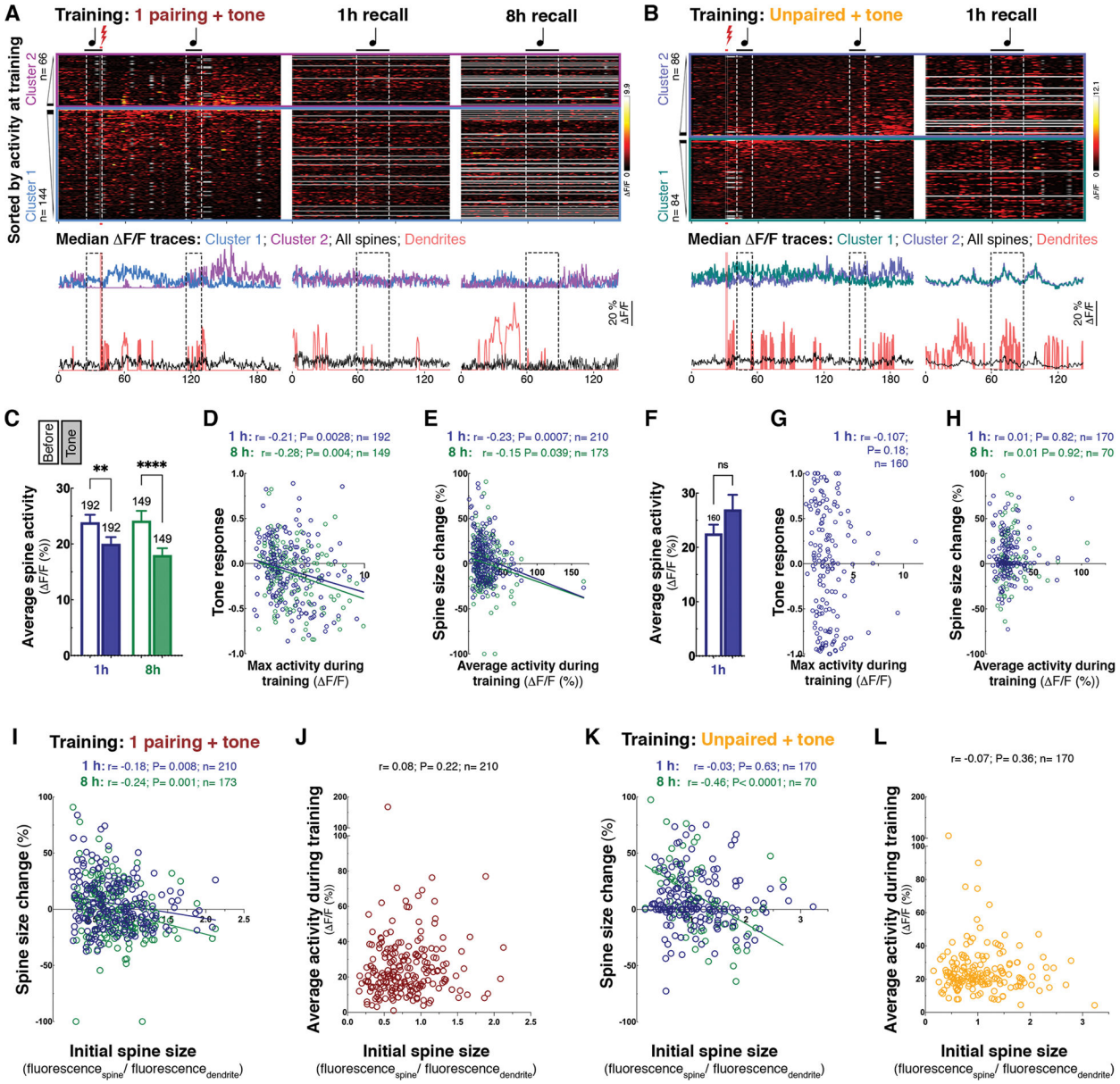

Figure 5. Persistent weakening of spines that were active during training

(A) Spine activity traces during training with the pairing + tone protocol and 1 & 8 h recall tests. Data are presented as a heat map (top) and median ΔF/F activity traces (bottom). NMF-based clustering identified two significant activity patterns during training. Spines of cluster one (n= 144/210; 9 L5 PNs) responded strongly to the shock, while spines of cluster two (n= 66) increased their activity following the presentation of the second tone. In the heat map, the spines' traces were sorted by cluster and total activity throughout training (most active towards the clusters' border). Activity during recalls is aligned according to training. Grey rows indicate missing data.

(B) Spine activity during non-associative training (unpaired + tone) and a 1 h recall test, depicted similar to as in A. Analysis spine activity revealed two significant clusters (84 and 86 spines from 7 cells).

(C) After associative training, spines exhibited negative tone responses at the 1 & 8 h recalls. **p= 0.004; ****p< 0.0001; paired t-test; n= 192 & 149 spine pairs; 9 cells.
(D, E) After associative training, tone responses at recalls (D), and spine size changes (E) correlated negatively with measures of activity during training. Pearson's correlation (192 and 149 spines in D; 210 and 173 spines in E; 9 cells).
(F) After non-associative training, spines did not exhibit a negative tone response at the 1 h recall test. paired t-test; n= 160 spine pairs; 7 cells.
(G, H) After non-associative training, tone responses at recall (G), and spine size changes (H) did not correlate with measures of activity during training. Pearson's correlation (160 spines in G; 170 and 70 spines in E; 4–7 cells).
(I-L) Indication of an activity-independent effect on spine size. After associative training, changes in spine size correlated negatively with initial spine size. Pearson's correlation (210 and 173 spines from 9 cells in I) This trend was also evident 8 h after non-associative training (70 spines from 4 cells in K). Note that activity during training did not correlate with initial spine size in both training regimes. Pearson's correlation (210 and 170 spines, from 9 and 7 cells, in J and L, respectively).
See also Figures S5, S6 and Video S4.

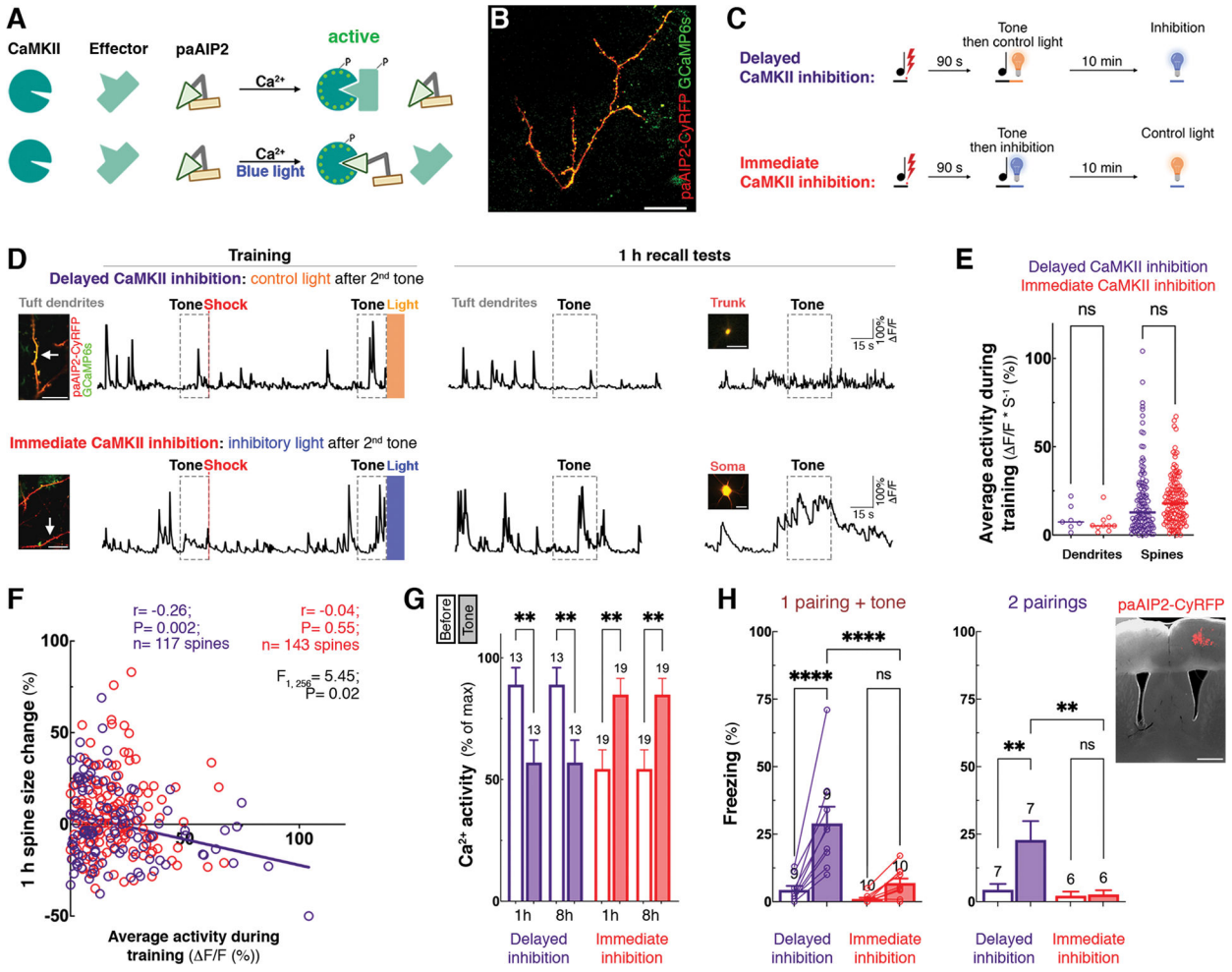

Figure 6. Disruption of CaMKII-dependent spine plasticity perturbed negative tone responses and conditioned freezing

(A) Schematics of CaMKII inhibition by paAIP2. Upon illumination (blue light, 470 nm), paAIP2 is relieved from autoinhibition to bind to active CaMKII, thus preventing it from activating downstream effectors.

(B) Sparse double labeling of PNs with paAIP2-CyRFP and GCaMP6s. This labeling approach enabled measuring changes in dendritic and spine activity while minimizing the disruption within the local circuit.

(C) Animals were trained with CaMKII inhibition immediately after the second tone or at a 10 min delay. A second light (orange) was used to control for the effects of illuminating the animals.

(D) Example ΔF/F traces of dendritic and somatic Ca^{2+} activities during associative training with immediate or delayed CaMKII inhibition, and 1 h recall tests. Immediate inhibition of CaMKII disrupted negative somatic responses to the tone at recall.

(E) During training, dendritic and spine activities during training were similar between the two groups. Activity was calculated for the entire training period (ns: not significant).

(F) Spines of the immediate inhibition group did not show a negative correlation between activity at training and plasticity. Plasticity between the two groups differed significantly; $F_{1,256}$= 5.45, p= 0.02; One-way ANCOVA.
(G) Dendrites and somata of the delayed inhibition group exhibited negative tone responses 1 and 8 h after training whereas those of the immediate inhibition group showed positive responses. (**p= 0.009; One-way ANOVA; Fisher's LSD test; n= 7 dendrites (of different cells) and 6 somata (delayed inhibition); 10 dendrites and 9 somata (immediate inhibition).
(H) Disruption of CaMKII-dependent plasticity perturbed conditioned freezing. M1 was labeled densely with paAIP2 (inset), and animals were trained 3 weeks later with the pairing + tone or two-parings protocol. CaMKII inhibition was in B (applied throughout the entire second pairing in the two-pairing condition). ****p< 0.0001; **p< 0.0035; One-way ANOVA; Fisher's LSD test; n= 6–10 animals per group.
Scale bars represent 50 μm in B, 20 μm in C, and 1 mm in H.
See also Figure S6 and Videos S4, S6.

Key resources table

REAGENT or RESOURCE	SOURCE	IDENTIFIER
Antibodies		
Bacterial and virus strains		
AAV9.CaMKII::Cre	Addgene	105551-AAV9
AAV9.FLEX.tdTomato	Addgene	28306-AAV9
AAV9.FLEX.CAG.GCaMP6s	Addgene	100842-AAV9
AAV5-FLEX-ArchT-tdTomato	Addgene	28305-AAV5
AAV9.synP.DIO.EGFP	Addgene	100043-AAV9
AAV1.DIO hSyn.hM4D(Gi)-mCherry	Addgene	44362-AAV9
AAV9.CamKII.GCaMP6s.WPRE.SV40	Addgene	107790-AAV9
AAV9.FLEX.CAG.paAIP2-CyRFP	This paper	
Biological samples		
Chemicals, peptides, and recombinant proteins		
Ketamine	Covetrus	Catalog number: VINV-CIII-0016
Xylazine	AnaSed	NDC: 59399-110-20
Meloxicam	Covetrus	NDC: 11695-6936-1
Lidocain2	Covetrus	NDC: 11695-4149-1
CNO	Millipore Sigma	CAS Number: 34233-69-7
Critical commercial assays		
Deposited data		
Experimental models: Cell lines		
Experimental models: Organisms/strains		
Mouse: *Thy1*-GCaMP6s	The Jackson Laboratory	Ref: 38
Ndnf-IRES-Cre	Rudy lab, available commercially	Stock Number: JAX:030757 Ref: 40
PValb $^{tm1(cre)Arbr}$	The Jackson Laboratory	Stock Number: JAX:017320
Sst$^{tm2.1(cre)Zjh}$	The Jackson Laboratory	Stock Number: JAX:013044

REAGENT or RESOURCE	SOURCE	IDENTIFIER
Oligonucleotides		
Recombinant DNA		
Software and algorithms		
MATLAB	MathWorks	https://www.mathworks.com/products/matlab.html
Other		

LIFE SCIENCE TABLE WITH EXAMPLES FOR AUTHOR REFERENCE

REAGENT or RESOURCE	SOURCE	IDENTIFIER
Antibodies		
Rabbit monoclonal anti-Snail	Cell Signaling Technology	Cat#3879S; RRID: AB_2255011
Mouse monoclonal anti-Tubulin (clone DM1A)	Sigma-Aldrich	Cat#T9026; RRID: AB_477593
Rabbit polyclonal anti-BMAL1	This paper	N/A
Bacterial and virus strains		
pAAV-hSyn-DIO-hM3D(Gq)-mCherry	Krashes et al.[1]	Addgene AAV5; 44361-AAV5
AAV5-EF1a-DIO-hChR2(H134R)-EYFP	Hope Center Viral Vectors Core	N/A
Cowpox virus Brighton Red	BEI Resources	NR-88
Zika-SMGC-1, GENBANK: KX266255	Isolated from patient (Wang et al.[2])	N/A
Staphylococcus aureus	ATCC	ATCC 29213
Streptococcus pyogenes: M1 serotype strain: strain SF370; M1 GAS	ATCC	ATCC 700294
Biological samples		
Healthy adult BA9 brain tissue	University of Maryland Brain & Tissue Bank; http://medschool.umaryland.edu/btbank/	Cat#UMB1455
Human hippocampal brain blocks	New York Brain Bank	http://nybb.hs.columbia.edu/
Patient-derived xenografts (PDX)	Children's Oncology Group Cell Culture and Xenograft Repository	http://cogcell.org/
Chemicals, peptides, and recombinant proteins		
MK-2206 AKT inhibitor	Selleck Chemicals	S1078; CAS: 1032350-13-2
SB-505124	Sigma-Aldrich	S4696; CAS: 694433-59-5 (free base)
Picrotoxin	Sigma-Aldrich	P1675; CAS: 124-87-8
Human TGF-β	R&D	240-B; GenPept: P01137
Activated S6K1	Millipore	Cat#14-486
GST-BMAL1	Novus	Cat#H00000406-P01
Critical commercial assays		
EasyTag EXPRESS 35S Protein Labeling Kit	PerkinElmer	NEG772014MC
CaspaseGlo 3/7	Promega	G8090
TruSeq ChIP Sample Prep Kit	Illumina	IP-202-1012
Deposited data		
Raw and analyzed data	This paper	GEO: GSE63473
B-RAF RBD (apo) structure	This paper	PDB: 5J17

REAGENT or RESOURCE	SOURCE	IDENTIFIER
Human reference genome NCBI build 37, GRCh37	Genome Reference Consortium	http://www.ncbi.nlm.nih.gov/projects/genome/assembly/grc/human/
Nanog STILT inference	This paper; Mendeley Data	http://dx.doi.org/10.17632/wx6s4mj7s8.2
Affinity-based mass spectrometry performed with 57 genes	This paper; Mendeley Data	Table S8; http://dx.doi.org/10.17632/5hvpvspw82.1
Experimental models: Cell lines		
Hamster: CHO cells	ATCC	CRL-11268
D. melanogaster: Cell line S2: S2-DRSC	Laboratory of Norbert Perrimon	FlyBase: FBtc0000181
Human: Passage 40 H9 ES cells	MSKCC stem cell core facility	N/A
Human: HUES 8 hESC line (NIH approval number NIHhESC-09-0021)	HSCI iPS Core	hES Cell Line: HUES-8
Experimental models: Organisms/strains		
C. elegans: Strain BC4011: srl-1(s2500) II; dpy-18(e364) III; unc-46(e177)rol-3(s1040) V.	Caenorhabditis Genetics Center	WB Strain: BC4011; WormBase: WBVar00241916
D. melanogaster: RNAi of Sxl: y[1] sc[*] v[1]; P{TRiP.HMS00609}attP2	Bloomington Drosophila Stock Center	BDSC:34393; FlyBase: FBtp0064874
S. cerevisiae: Strain background: W303	ATCC	ATTC: 208353
Mouse: R6/2: B6CBA-Tg(HDexon1)62Gpb/3J	The Jackson Laboratory	JAX: 006494
Mouse: OXTRfl/fl: B6.129(SJL)-Oxtr$^{tm1.1Wsy}$/J	The Jackson Laboratory	RRID: IMSR_JAX:008471
Zebrafish: Tg(Shha:GFP)t10: t10Tg	Neumann and Nuesslein-Volhard[3]	ZFIN: ZDB-GENO-060207-1
Arabidopsis: 35S::PIF4-YFP, BZR1-CFP	Wang et al.[4]	N/A
Arabidopsis: JYB1021.2: pS24(AT5G58010)::cS24:GFP(-G):NOS #1	NASC	NASC ID: N70450
Oligonucleotides		
siRNA targeting sequence: PIP5K I alpha #1: ACACAGUACUCAGUUGAUA	This paper	N/A
Primers for XX, see Table SX	This paper	N/A
Primer: GFP/YFP/CFP Forward: GCACGACTTCTTCAAGTCCGCCATGCC	This paper	N/A
Morpholino: MO-pax2a GGTCTGCTTTGCAGTGAATATCCAT	Gene Tools	ZFIN: ZDB-MRPHLNO-061106-5
ACTB (hs01060665_g1)	Life Technologies	Cat#4331182
RNA sequence: hnRNPA1_ligand: UAGGGACUUAGGGUUCUCUCUAGGGACUUAGGGUUCUCUCUAGGGA	This paper	N/A
Recombinant DNA		
pLVX-Tight-Puro (TetOn)	Clonetech	Cat#632162
Plasmid: GFP-Nito	This paper	N/A
cDNA GH111110	Drosophila Genomics Resource Center	DGRC:5666; FlyBase:FBcl0130415
AAV2/1-hsyn-GCaMP6- WPRE	Chen et al.[5]	N/A
Mouse raptor: pLKO mouse shRNA 1 raptor	Thoreen et al.[6]	Addgene Plasmid #21339

REAGENT or RESOURCE	SOURCE	IDENTIFIER
Software and algorithms		
ImageJ	Schneider et al.[7]	https://imagej.nih.gov/ij/
Bowtie2	Langmead and Salzberg[8]	http://bowtie-bio.sourceforge.net/bowtie2/index.shtml
Samtools	Li et al.[9]	http://samtools.sourceforge.net/
Weighted Maximal Information Component Analysis v0.9	Rau et al.[10]	https://github.com/ChristophRau/wMICA
ICS algorithm	This paper; Mendeley Data	http://dx.doi.org/10.17632/5hvpvspw82.1
Other		
Sequence data, analyses, and resources related to the ultra-deep sequencing of the AML31 tumor, relapse, and matched normal	This paper	http://aml31.genome.wustl.edu
Resource website for the AML31 publication	This paper	https://github.com/chrisamiller/aml31SuppSite

PHYSICAL SCIENCE TABLE WITH EXAMPLES FOR AUTHOR REFERENCE

REAGENT or RESOURCE	SOURCE	IDENTIFIER
Chemicals, peptides, and recombinant proteins		
QD605 streptavidin conjugated quantum dot	Thermo Fisher Scientific	Cat#Q10101MP
Platinum black	Sigma-Aldrich	Cat#205915
Sodium formate BioUltra, ≥99.0% (NT)	Sigma-Aldrich	Cat#71359
Chloramphenicol	Sigma-Aldrich	Cat#C0378
Carbon dioxide (^{13}C, 99%) (<2% ^{18}O)	Cambridge Isotope Laboratories	CLM-185-5
Poly(vinylidene fluoride-co-hexafluoropropylene)	Sigma-Aldrich	427179
PTFE Hydrophilic Membrane Filters, 0.22 μm, 90 mm	Scientificfilters.com/Tisch Scientific	SF13842
Critical commercial assays		
Folic Acid (FA) ELISA kit	Alpha Diagnostic International	Cat# 0365-0B9
TMT10plex Isobaric Label Reagent Set	Thermo Fisher	A37725
Surface Plasmon Resonance CM5 kit	GE Healthcare	Cat#29104988
NanoBRET Target Engagement K-5 kit	Promega	Cat#N2500
Deposited data		
B-RAF RBD (apo) structure	This paper	PDB: 5J17
Structure of compound 5	This paper; Cambridge Crystallographic Data Center	CCDC: 2016466
Code for constraints-based modeling and analysis of autotrophic *E. coli*	This paper	https://gitlab.com/elad.noor/sloppy/tree/master/rubisco
Software and algorithms		
Gaussian09	Frish et al.[1]	https://gaussian.com
Python version 2.7	Python Software Foundation	https://www.python.org
ChemDraw Professional 18.0	PerkinElmer	https://www.perkinelmer.com/category/chemdraw
Weighted Maximal Information Component Analysis v0.9	Rau et al.[2]	https://github.com/ChristophRau/wMICA
Other		
DASGIP MX4/4 Gas Mixing Module for 4 Vessels with a Mass Flow Controller	Eppendorf	Cat#76DGMX44
Agilent 1200 series HPLC	Agilent Technologies	https://www.agilent.com/en/products/liquid-chromatography
PHI Quantera II XPS	ULVAC-PHI, Inc.	https://www.ulvac-phi.com/en/products/xps/phi-quantera-ii/